# Impact of soil erosion voids on reinforced concrete pipe responses to surface loads

Chapman, David; Peter, Jane; Moore, Ian; Hoult, Neil

*DOI:*
10.1016/j.tust.2018.08.003



*Document Version*
Peer reviewed version

*Citation for published version (Harvard):*
Chapman, D, Peter, J, Moore, I & Hoult, N 2018, 'Impact of soil erosion voids on reinforced concrete pipe responses to surface loads', *Tunnelling and Underground Space Technology*, vol. 82, pp. 111-124. https://doi.org/10.1016/j.tust.2018.08.003

# Manuscript Details

| | |
|---|---|
| **Manuscript number** | TUST_2017_841_R1 |
| **Title** | Impact of soil erosion voids on reinforced concrete pipe responses to surface loads |
| **Article type** | Research Paper |


**Abstract**

This paper discusses the results of controlled, full-scale laboratory experiments on 0.9 m (36 in.) internal diameter reinforced concrete pipes (RC pipes) in the presence of simulated erosion voids. This study introduces a novel, yet practical, experimental method to simulate erosion voids near buried pipes. Using this method, the paper focuses on capturing the circumferential moment changes experienced by a 0.9 m (36 in.) internal diameter RC pipe buried at 0.9 m depth as voids of different sizes (approximate cross-sectional areas of 0.16 m2 and 0.31 m2) develop beside it, which have not been investigated before in such tests. The tests were also repeated after the erosion voids were repaired using a low strength grout (~ 2MPa) to characterize it as a potential rehabilitation solution, and the moment changes were recorded. The presence of erosion voids resulted in an overall increase in bending moment with the invert moments being affected the most (e.g., 70% increase in the invert moment between the intact soil result and the small void result and a 26% increase in the invert moment between the intact soil result and the extrapolated large void results). While, grouting the erosion voids resulted in an overall improvement in the pipe responses, there was still a 50% increase in the invert moment between the intact soil result and the grouted small void result and a 22% change between the grouted large void and the intact soil tests). The large void tests showed that soil collapse is the dominant failure mechanism at high loads. Comparing the modified bedding factor values for pipes with different void sizes and void condition (pre- and post-grouting), the intact soil always featured the highest bedding factor, followed by grouted large void (approximately 22% reduction in bedding factor), grouted small void (approximately 36% reduction), and small void before grouting (approximately 39% reduction).



| | |
|---|---|
| **Keywords** | erosion voids; concrete pipes; rehabilitation; grouting |



| | |
|---|---|
| **Corresponding Author** | Neil Hoult |
| **Corresponding Author's Institution** | Queen's University |
| **Order of Authors** | Jane Peter, David Chapman, Ian Moore, Neil Hoult |


| | |
|---|---|
| **Suggested reviewers** | Timothy McGrath, Ece Erdogmus, Ming Xu, David Becerril Garcia, Michael Katona |

**Highlights**

- Erosion voids at the springlines cause pipes to crack at lower loads.
- Erosion voids resulted in an overall increase in bending moments especially at invert.
- Ultimate capacity of pipes with larger voids controlled by soil collapse.
- Bedding factor values depend heavily on degree of compaction.

# Impact of soil erosion voids on reinforced concrete pipe responses to surface loads

Jane M. Peter [a], Dr. David Chapman [b], Dr. Ian D. Moore [c], and Dr. Neil Hoult [d]

[a] Doctoral candidate, Queen's University, Kingston, ON, Canada K7L 3N6. Email: jane.peter@queensu.ca

[b] Ph.D., CEng, Professor of Geotechnical and Underground Engineering, University of Birmingham, Edgbaston, Birmingham, UK B15 2TT. Email: d.n.chapman@bham.ac.uk

[c] Ph.D., PEng, Professor and Canada Research Chair in Infrastructure Engineering, GeoEngineering Centre at Queen's – RMC, Queen's University, Kingston, ON, Canada K7L 3N6. Email: ian.moore@queensu.ca

[d] Ph.D., PEng, Associate Professor, Queen's University, ON, Canada K7L 3N6. Email: neil.hoult@queensu.ca (corresponding author)

**Abstract**

This paper discusses the results of controlled, full-scale laboratory experiments on 0.9 m (36 in.) internal diameter reinforced concrete pipes (RC pipes) in the presence of simulated erosion voids. This study introduces a novel, yet practical, experimental method to simulate erosion voids near buried pipes. Using this method, the paper focuses on capturing the circumferential moment changes experienced by a 0.9 m (36 in.) internal diameter RC pipe buried at 0.9 m depth as voids of different sizes (approximate cross-sectional areas of 0.16 $m^2$ and 0.31 $m^2$) develop beside it, which have not been investigated before in such tests. The tests were also repeated after the erosion voids were repaired using a low strength grout (~ 2MPa) to characterize it as a potential rehabilitation solution, and the moment changes were recorded. The presence of erosion voids resulted in an overall increase in bending moment with the invert moments being affected the most (e.g., 70% increase in the invert moment between the intact soil result and the small void result and a 26% increase in the invert moment between the intact soil result and the

extrapolated large void results). While, grouting the erosion voids resulted in an overall improvement in the pipe responses, there was still a 50% increase in the invert moment between the intact soil result and the grouted small void result and a 22% change between the grouted large void and the intact soil tests). The large void tests showed that soil collapse is the dominant failure mechanism at high loads. Comparing the modified bedding factor values for pipes with different void sizes and void condition (pre- and post-grouting), the intact soil always featured the highest bedding factor, followed by grouted large void (approximately 22% reduction in bedding factor), grouted small void (approximately 36% reduction), and small void before grouting (approximately 39% reduction).

**Keywords:** erosion voids; concrete pipes; rehabilitation; grouting

## 1.0 Introduction

According to McGrath *et al.,* (1999), the longevity of a pipe relies heavily on the pipe-soil interaction. However, over time, reinforced concrete pipes (RC pipes) develop issues such as cracks, leaking joints, or experience misalignment from rotation and movements (Moore, 2008). These issues contribute to groundwater infiltration that causes smaller soil particles in the backfill to be washed away causing erosion voids to develop.

The presence of erosion voids next to pipes removes soil support at that location, which can result in uneven load spreading in the ground surrounding the pipe (Tan and Moore, 2007; Balkaya *et al.,* 2013). A rigid pipe, such as an RC pipe, resists surface loads in bending and shows negative arching, where surface load is attracted to the pipe by virtue of its higher stiffness compared to the soil it replaced (Young and Trott, 1984). The loss of soil support during the formation of erosion voids affects the soil-pipe interaction and has the potential to increase

50 the bending moments in the pipe, which could lead to failure of the system if the erosion voids
51 are large enough. Hence, it is necessary to address questions such as how do voids influence soil-
52 pipe interaction, do voids increase the live load bending moments in the pipes, what is the effect
53 of void size on bending moments, and can grouting of the void restore the 'intact soil' strength?

54 Previous finite element studies have investigated surface load transfer to buried pipes
55 when there were erosion voids in the backfill. For example, Tan and Moore (2007) calculated an
56 increase in the bending moments in rigid pipes with erosion voids located beside the pipe
57 springlines (see also Tan, 2007). For the assumptions associated with their elastic-plastic finite
58 element modeling and voids with circular boundaries, they show that void location beside the
59 springline causes earth load bending moment in the pipe to increase, and for voids under the
60 invert or over the crown to decrease. The deterioration of the soil support can in fact result in the
61 pipe reaching its performance limits before the end of its design life. In addition, groundwater
62 infiltration can have other undesirable effects if left unattended including negative hydraulic
63 impacts, spills, sinkhole formation, and therefore disruption to traffic or loss of life. One
64 potential method of mitigating these issues is to grout the erosion voids, however no
65 experimental work has been undertaken to investigate the performance of a rigid pipe with
66 grouted erosion voids.

67 Pipe design equations consider intact soil support surrounding a buried pipe, and recently
68 MacDougall et al. (2016) reported on an experimental study to quantify concrete pipe response
69 and evaluate the performance of reinforced concrete pipe design for 'intact ground' (where no
70 erosion void has developed). Peter and Moore (2018) report on full-scale experiments to quantify
71 the effect of an erosion void on the response of a corrugated steel pipe under surface live load,
72 and no full-scale experiments have examined the effect of erosion voids on rigid pipes.

One final challenge associated with erosion voids and rehabilitated erosion voids is how to quantify their impact on the capacity of the pipe. Currently, bedding factors are used in the Indirect Design method to relate the behaviour of a concrete pipe when buried to the results of a D-load or three edge bearing test (ASTM C497-16a). Thus, a potential method of accounting for the presence of erosion voids would be to develop modified bedding factors that would account for the effects of the reduced soil support.

In light of this background, this paper reports the outcomes of a full-scale experimental study conducted on 0.9 m (36 in.) diameter reinforced concrete pipes with simulated erosion voids. The objectives of the paper are to (i) measure the difference in pipe bending moments for pipes with and without erosion voids, (ii) measure the difference in bending moments for pipes with and without grouted voids, and (iii) use these experimentally measured bending moments to develop modified surface load bedding factors for pipes with erosion voids and grouted erosion voids.

## 2.0 Background

### 2.1 Void geometry

El-Taher and Moore (2008) looked at the influence of erosion voids on the yielding and buckling failure of corroded metal culverts using finite element analysis. They found that in the presence of an erosion void, the moments were more affected than the thrust in the pipe. Additionally, moment (the controlling factor for rigid pipes), was affected by both changes in the position of the erosion void with respect to the pipe and the volume of the void.

94 The void location on the circumference of the pipe considered in the current study is
95 based on the work of two previous investigations. Firstly, the numerical study presented by Tan
96 and Moore (2007) considered erosion voids at the invert of a rigid pipe that resulted in a decrease
97 in the magnitude of the overall bending moments experienced by the pipe. However, the
98 presence of an erosion void at the springline was the most critical as it resulted in an increase in
99 the magnitude of bending moments at all critical locations (i.e. crown, invert, and springlines).
100 As a result, the void in the present study was simulated at the springlines to capture the critical
101 changes in bending moments around the pipe circumference. Secondly, the first study by
102 Spasojevic et al., (2007) found that although a common location for voids is under the invert due
103 to fluids leaking from drainage and sewer pipes, these voids are unstable since the soil around
104 the springlines tends to collapse and fill the void at the invert.

105 Obtaining images of erosion voids is challenging and hence replicating their true
106 geometry is difficult. However, drawing on the geometry considered in Tan and Moore (2007),
107 El-Taher and Moore (2008), and Balkaya *et al.* (2012), the erosion void was represented as a
108 prismatic arc shape running along the length of the pipe on one side, thus making it a 2-D
109 problem. Furthermore, Balkaya *et al.,* (2012) studied the stresses and deformations in a PVC
110 water pipe with different void geometries at the invert and haunches located at the joints using
111 finite element analysis and found that joint rotation was magnified when voids were present at
112 the joints. This study was validated by Becerril and Moore (2014) using full-scale experiments.
113 Hence, in order to avoid this complexity and to focus on the impact of erosion voids on pipe
114 strength, the voids in the present study were represented only along the length of the pipe barrel.

115 In addition, Tan and Moore (2007) showed that the contact angle of erosion voids plays a
116 dominant role in stress changes. Hence, in the present study different sizes of voids were also
117 considered.

118 **2.2 Soil cover**

119 Lay and Brachman (2013) looked at the response of a RC pipe to surface live loads in an
120 intact soil condition using full-scale experiments. RC pipes showed only 50-60% of cracking
121 strain at nominal loads. As a result, no cracking developed in the pipe when it was subjected to
122 CL-625 single-axle truck loading at nominal loads. It was also found that increasing the soil
123 cover caused a reduction in the crown bending moment due to load spreading and arching.
124 Hence, a minimum cover depth to diameter ratio of one was selected for the present study.

125 **2.3 Accuracy of bedding factors**

126 Indirect design of buried concrete pipes uses a quantity called the Bedding Factor.
127 Bedding factors were originally defined as the load per unit length along the pipe crown that
128 induced the limiting crack (width of 0.25 mm) in a D-load test divided by the load that induced
129 the limiting crack when the pipe was buried. This will subsequently be referred to as the
130 'moment resistance' Bedding factor, since it relates to load that induces the design limit state in
131 the pipe. However, until the recent work of MacDougall et al. (2016), there were no experiments
132 performed where crack width was measured for tests on buried pipes. Therefore, the Bedding
133 factor has been quantified considering the ratio of moment induced under vertical loads in a three
134 edge bearing test on the pipe in a laboratory, to the moment that develops in the same pipe under
135 the same level of vertical load in the field when it is buried. This will be subsequently be referred

to as the 'moment demand' bedding factor, since it is calculated using the moment demands in the pipe at loads below any design limit state.

The Bedding factor is greater than 1 (and the bending moments in the buried pipe decrease relative to those in the three edge bearing test) since the soil around the pipe spreads load across the top and bottom of the pipe, and lateral earth pressures develop that counteract the moments from the vertical loading. MacDougall *et al.* (2016) used tests on 0.6 m and 1.2 m diameter pipes at shallow cover to show that for those structures, the Indirect Design method gives conservative solutions when designing RC pipes and this could mean that reinforced concrete pipes already have the necessary reserve capacity to negate the effects of an erosion void beside a pipe. Since the Indirect Design method represents the most common approach used in pipe design across North America, the effect of erosion voids on Bedding Factors will be used to quantify the resulting changes in pipe capacity.

## 3.0 Methods

### 3.1 Introduction

In order to achieve the objectives of the study, seven full-scale buried experiments using 0.9 m (36 in) internal diameter RC pipes were conducted with and without simulated erosion voids. This section initially describes the testing arrangement and setup, followed by details of the individual components, i.e. the pipe, the soil, the erosion voids, and the grout.

### 3.2 Testing regime

Table 1 provides a summary of the specimens tested during the study. The first specimen was tested in three edge bearing (D-load; ASTM C497-16a). The buried pipe experiments were conducted in pairs since two pipe specimens could be buried simultaneously in the test facility.

158 Since the pipe response to the wheel pair load was used (featuring a small contact area and
159 limited load spreading along the pipes), and since rubber gaskets were not inserted between the
160 two pipe specimens, the two pipes responded independently, and hence they have been treated as
161 individual specimens. This was confirmed using the strain gauge readings on the specimen
162 adjacent to the one being tested, which showed no significant changes in strains as loads were
163 applied over the other specimen. As such, specimens 2 and 3 were buried at the same time, as
164 were specimens 4 and 5, and finally specimens 6 and 7.

165 Table 1: Test details

| **Specimen** | **Test description** | **Loading limit** |
|---|---|---|
| 1 | D-load (three edge bearing) test | Onset of crack at 196 kN |
| 2 | Intact soil (80-85% Standard Proctor) | Onset of crack at 274 kN |
| 3 | Grouted small void (80-85% Standard Proctor) | Onset of crack at 308 kN |
| 4 | Small void (80-85% Standard Proctor) | Onset of crack at 277 kN |
| 5 | Large void (80-85% Standard Proctor) | Soil collapse at ~ 250 kN |
| 6 | Intact soil (90-95% Standard proctor) | Onset of crack at 525 kN |

| | | |
|---|---|---|
| 7a | Large void (90-95% Standard Proctor) | Tested only up to 50 kN as the void was grouted and tested as specimen 7b. |
| 7b | Grouted large void (90-95% Standard Proctor) | Did not crack and instead observed soil collapse in the first factored service load cycle (128.3 kN) and a misalignment in the actuator. |

166

167 Specimen 1 was tested according to ASTM C497-16a until a maximum allowable crack
168 width of 0.25 mm (0.01 in.) crack width was achieved. The D-load test setup and dimensions can
169 be seen in Figure 1. Load was applied using a 2000 kN (450 kips) actuator seated directly on top
170 of an I-beam. After the D-load test, the pipe was cut into two segments and used as the end pipes
171 in the subsequent burial tests.

172 Specimen 2 was a pipe section buried in an intact soil condition and specimen 3 was a
173 pipe section with a grouted small void (see Figures 2 and 3). Installation type 3 using a
174 compaction of 80-85% Standard Proctor was adopted for both of these tests (AASHTO LRFD,
175 2012). This installation type was used to represent backfill that had deteriorated over time
176 (Moore *et al.*, 2012). The void for specimen 3 was simulated using an air bladder that was
177 inflated and tied to the sides of the pipe, then punctured after burial, and filled with grout as
178 discussed in sections 3.2.2 and 3.2.3 (the method of simulating an erosion void using an air
179 bladder was developed during the earlier testing project on corrugated steel pipe culvert reported
180 by Peter and Moore, 2018).

181 Specimen 4 was buried with a smaller simulated erosion void at the springline, and
182 specimen 5 featured a larger erosion void (see Figure 4). The dimensions of these voids are

183 defined in a subsequent section. The same level of compaction was used as specimens 2 and 3 to
184 simulate deteriorated backfill (Moore *et al.*, 2012).

185 Specimen 6 also had intact soil but with installation type 2 with a compaction of 90-95%
186 Standard Proctor (AASHTO LRFD, 2012); it was used to investigate the performance of
187 reinforced concrete pipes in well compacted soil. Specimen 7 was the companion for specimen 6
188 and was tested with a large void, under installation type 2, for service loads up to 50 kN. The
189 large void (specimen 7a) was later grouted (and denoted specimen 7b) and tested under service
190 loads (up to 50 kN) and up to a maximum possible test load (either cracking in the pipe or soil
191 failure). Here, 'soil failure' is intended to mean collapse associated with a mechanism (i.e. what
192 is referred to as 'general shear failure' by Lambe and Whitman (1979), rather than just shear
193 failure at a point).

194 Each buried pipe specimen was initially loaded using a simulated wheel pair up to a load
195 of 50 kN or 113.4 kN (for specimens with and without erosion voids, respectively), before being
196 loaded up to the maximum possible load as discussed in section 3.6.

197 **3.3 Sample description**

198 **3.3.1 Reinforced concrete pipes**

199 The tests were conducted using seven Class III (65-D) reinforced concrete pipes with 0.9
200 m internal diameter, 2.4 m length, and 121 mm wall thickness (denoted by the Wall C
201 configuration defined in ASTM C497-16a). The outer diameter at the bell measured 1.3 m.
202 These pipes are normally used in culvert, storm sewer and sanitary sewer applications. The
203 concrete and steel material properties were not supplied by the manufacturer, however, since the

response of the pipes was in the uncracked linear elastic region for most of the testing, the flexural stiffness of the pipes can be determined using the method outlined in section 4.1.

### 3.3.2 Erosion voids

The erosion voids were simulated using air bladders attached to the pipes. The small air bladder had a length of 1.9 m, width of 0.74 m, thickness of 0.22 m, and a cross-sectional area of 0.16 $m^2$ (Figure 5). The width of the air bladder wrapped around the circumference of the pipe, so that it was in contact with the exterior barrel of the pipe over an angle of approximately 40 degrees. The larger air bladder had a length of 1.9 m, width of 1.4 m, thickness of 0.22 m with a cross sectional area of 0.31 $m^2$ (Figure 5), contacting the pipe exterior over an angle of about 70 degrees). The bladder position and its shape were maintained and protected with an overlay of geotextile (see Figure 3).

As discussed in section 2, the most critical location for erosion voids to form is around the springlines of the pipe. Hence, the small air bladder spanned from the haunch to just above the springline, while the larger air bladder spanned from the haunch to the crown of the outside circumference of the pipe (Figure 5). The void geometry chosen was a prismatic arc that ran along the length of the pipe; therefore, the experiments undertaken in this study could be considered as involving approximately a plane strain pipe response, with longitudinal effects being negligible. While this representative geometry is not necessarily similar to the one that would occur if erosion resulted from joint leakage, it is considered a useful approximation for this first study on void effects.

The degree of soil compaction and soil suction may have offered the necessary resistance to retain the void shapes and prevent initial collapse of the erosion voids before testing under

surface load. This was reconfirmed in Peter and Moore (2018) based on the excavated geometry of the grouted specimen.

### 3.4 Backfill

As seen in Figure 3, the specimens were placed on a well-compacted bedding. Small pits were excavated prior to placing the pipe on the bedding to accommodate the protrusion of the bell on each pipe. A flexible retaining wall assembled from steel mesh and geosynthetic was used as the south end wall next to the concrete retaining blocks as seen in the elevation drawings in Figures 2 and 4. The steel mesh extended 1000 mm into the soil at each lift to prevent collapse (this system has been used at Queen's University in many prior buried pipe experiments, e.g. Becerril García and Moore, 2013 and 2014 a and b).

The backfill material used in the tests was a well graded, granular A sand, with fine to coarse grade materials (GW-SW soil according to the Unified Soil Classification System or as an AASHTO (2009) A-1 material) with a unit weight of 22kN/m$^3$ (Brachman *et al.*, 2010). The backfill was placed in nine 300 mm lifts to ensure the burial was consistent with depth and compacted using a vibrating plate tamper. Once the lifts were compacted, the dry density, water content, and percentage Standard Proctor were recorded using a CPN MC-1DR-P Portaprobe nuclear densometer (according to ASTM D6938-10). A minimum specified cover height of one diameter (i.e. 0.9 m) was used.

### 3.5 Grouting

A low strength foam grout (density 703 kg/m$^3$) was used to fill the voids in a single lift. The grout had a 7-day unconfined compressive strength of approximately 2.0 MPa. The mix was

prepared by volume and included Type III Portland cement, water, and a foaming agent (Aerix light by Euclid Chemical, Canada). Between the pipe and the air bladder, a vertical pipe was placed to allow the grout to enter into the simulated void. The end of the vertical pipe was placed close to the bottom of the void to ensure the void was completely filled. A narrow pipe (overflow pipe) was placed parallel to the pipe axis at the top of the void to monitor the grout level in the void. After backfilling, the air bladder was ruptured by drilling into it from the inside of the pipe. The air was allowed to escape through the holes for a period of several hours and the strains in the pipe were monitored during this period. After testing of the unrepaired structure was completed, the grout was carefully poured into the void using the vertical standpipe. Due to the porous nature of the grout and its low viscosity, the void filled readily. Grouting was stopped once the grout was observed to come out of the overflow pipe and it had filled the bottom half of the vertical grouting pipe.

### 3.6 Instrumentation

To measure the circumferential strains around the specimens, 16 strain gauges (of 51 mm (2 in.) length) (Figure 6) manufactured by Vishay Micro-Measurements Co. were used. The size of the strain gauges was chosen to be at least three times the size of the largest aggregate in the concrete to record average strains. The gauges were placed at critical locations around the pipes inner and outer circumference or extreme fibre surface locations (i.e. crown, invert, springlines, shoulder, and haunches). The axial positions of this and other instrumentations relative to the applied surface loads are defined in section 3.7.

In addition to using strain gauges, fibre optic strain sensors (FOS) were used to capture the complete circumferential strain profile around the specimen (Figure 6). Nylon coated fibre optic cables were glued to the inside and outside surfaces of the concrete pipes in two loops as

per the installation procedure outlined in Simpson *et al.,* (2015). The gauge length within the fibre was specified as 5 cm (similar to the conventional strain gauges) and spaced at 5 cm along the length of the cable.

Reliable estimates of curvature and bending moments prior to cracking were calculated using strain readings from strain gauges or fibre optics. Strain gauges and optical fibres were placed directly on the surface of the RC pipes. This type of application has been successfully used at Queen's University in many rigid pipe experiments, e.g. MacDougall *et al.*, (2016), and Moore *et al.*, (2012).

Diameter changes under surface loading were also measured using Linear Potentiometers (LP's) (Figure 6). Two LP's were placed inside the pipe directly under the centre of the wheel pad to measure the vertical and horizontal changes in the diameter as the ground above the pipes was loaded.

Two digital single lens reflex (DSLR) cameras were also set up to record the development of cracks at the crown and at the invert inside the pipes during loading using Particle Image Velocimetry (PIV) patches (Figure 6), but to manage the length of this article, the analysis procedures and crack-width data will be presented elsewhere.

The movement of the surface of the soil was also monitored using a servo-controlled Leica total station. Reflective prisms were used to capture the surface movement potentially occurring during loading (Figure 7). The prisms were located on a grid pattern of 450 mm spacing to cover an estimated zone of influence. No significant changes were observed in the target locations during testing and hence the results are not discussed in this paper.

### 3.7 Loading regime

For specimen 1 (D-load test, Figure 1), the load was increased using stroke control at 3 mm/min. In the buried pipe tests, the loads were applied using the same 2000 kN hydraulic actuator acting onto a loading pad. Service load tests used a steel pad dimensioned to the size of a standard AASHTO wheel pair of a design truck (254 mm x 508 mm – Figure 7). The maximum load test used larger wooden loading pad that measured 370 mm x 950 mm (Figure 7) to avoid premature soil collapse of the unpaved surface.

The fibre optics and strain gauges were positioned on the pipe surface directly under the corresponding location of surface load application, around three rings. One ring of fibre optics in the RC pipe was positioned at the approximate centreline of the load pad. At 254 mm on either side of the centreline (i.e. the edges of the load pad), a ring of strain gauges or a second ring of fibre optics was attached.

Three cycles of loading and unloading were conducted as part of the service load test (using the smaller loading pad) and one cycle of loading was conducted for the maximum load state test for each buried condition (using the larger wheel pad). The load was increased in steps and was held constant when the fibre optic strains were being recorded. In the service load tests, the loads were increased to 113.4 kN for tests 2, 3, 6, and 7b, but only to 50 kN for specimens 4, 5, and 7a (the small and large void) so as to prevent void collapse. In the maximum load tests, once the full design service load step was achieved, the load was increased in 10 kN increments until either a crack width in the RC pipe of 0.25 mm (a service limit defined for reinforecd concrete pipes by AASHTO, 2016) was observed at the inside crown or invert, or soil collapse of the surface occurred (observed visually).

## 4.0 Results and Discussion

### 4.1 Introduction

The following section presents the results of the experimental campaign. To understand the impact of burial (section 4.2), erosion voids (section 4.3), grouted voids (section 4.4), pipe cracking responses and linearity (section 4.5), and modified bedding factors (section 4.6) on the behaviour of reinforced concrete pipes, the fibre optic strain measurements were used to calculate curvatures, $\kappa$, using equation 1.

$$\kappa = \frac{\varepsilon_{inside} - \varepsilon_{outside}}{h} \quad (1)$$

Equation 2 was then used to calculate approximate values of the circumferential bending moments, $M$.

$$M = EI\kappa \times 10^{-3}\, Nm \quad (2)$$

where $\varepsilon_{inside}$ = the circumferential strain measured on the inside face of the pipe

$\varepsilon_{outside}$ = the circumferential strain measure on the outside face of the pipe

$h$ = pipe wall thickness = 121 mm

The material properties of the pipe were not supplied by the manufacturer. However, the flexural stiffness, EI, can be calculated using the experimental data by rearranging equation (2) to solve for EI and inputting the solution for the D-load moments proposed by Heger (1962) and the measured curvature. However, it is worth noting that the moment distribution for the D-load test (Figure 8) did not match the expected moment distribution (Heger, 1962). This is likely due to the D-load test setup used as seen in Figure 1. In this case, the top loading condition involves a

single point load being applied to the specimen through a steel beam, which is less stiff than the pipe itself resulting in a concentration of load in the pipe near the actuator. The bottom support condition involves a beam placed on top of compacted soil, which is stiffer than the pipe and results in load spreading along the length of the pipe. As such, the strains measured at the crown are not representative of the full pipe behaviour and so to calculate EI, the moment and curvatures at the invert were used. The equation for moment at the invert in an uncracked pipe is given in equation (3)(Heger, 1962).

$$M = 0.28\,\mathrm{Pr} \tag{3}$$

where P is the point load applied at the top of the pipe (100 kN for the D-load test) and r is the pipe radius (0.510 m). Using this moment and the curvature measured at the invert at an applied load of 100 kN, the flexural stiffness, EI, can be calculated as $7.73 \times 10^{12}$ Nmm$^2$. This value can be used to convert the curvatures calculated from the strains into moments. These equations are used under the assumption that the strain is linear through the wall thickness prior to cracking.

### 4.2 Impact of burial

Figure 8 compares the results from the D-load sample (specimen 1) to the intact soil test with the type 2 installation (specimen 6) to investigate the impact of burial in soil on pipe behaviour. To compare these two results, the strains and then circumferential bending moments in different pipes at the same equivalent load per unit length along the pipe axis had to be evaluated. For specimen 1, this load was determined by taking the total applied load and dividing by the length of the pipe to get an equivalent line load (in N/m). For specimen 6, the concept of the load spreading prism from the AASHTO LRFD (2012) design procedure were used to turn the load applied at the surface into an equivalent line load along the length of the pipe (to the

crown). For a burial depth of $H$ to the pipe crown and loading pad of width $W_0$ and length $L_0$, load per unit length along the buried pipe $F_H$ is given by Wang and Moore (2015) as:

$$F_H = \frac{wP_L}{L_0 + LLDF \times H} \tag{4}$$

(3)

where $P_L$ = the surface force on the loading pad

LLDF = the AASHTO LRFD, 2012, live load distribution factor (and equal to 1.15 for the coarse grained soils used in this study)

$w$ = the proportion of the load acting across the pipe barrel of outside diameter OD, where *'w'* is given by:

$$w = \min\begin{cases} \dfrac{OD}{W_0 + LLDF \times H} \\ 1 \end{cases} \tag{5}$$

Strains or moments can be compared directly if obtained at the same value of load ($F_H$) applied using the steel or wooden load pads. The strains in the D-load test were compared to the strains in the buried pipe test when the forces per unit length ($F_H$) on the two pipes were similar. The response of the RC pipes is assumed to be linear and elastic up to the point of first cracking. As a result, the D-load strains compared in Figure 8 were scaled from the closest $F_H$ to compare to the equivalent force per unit length ($F_H$) in the buried pipe. Figure 8 is the first of a series of radial plots that are used to quantify how soil support influences live load bending moments.

375 Strains measured on the tension side of the concrete wall were positive and strains measured on
376 the compression side were negative.

377 Figure 8 shows the moment for the D-load test plotted using results extrapolated from
378 100 kN to 110.16 kN, so they correspond to the same $F_H$ as the intact soil test. The moments
379 increased linearly with load from 20 kN to 120 kN (further discussed in section 4.5); hence, the
380 extrapolated results are considered reliable. From Figure 8, it can be seen that the moments in the
381 D-load test are approximately 9 times higher at the crown, 3.3 times higher at the invert, and 4
382 times higher at the springline locations compared to the intact soil responses (specimen 6). This
383 reduction in moment magnitude when the pipe is buried is due to the effect of the soil and
384 illustrates the basis for the Bedding Factor ($B_f$) that will be discussed in detail in section 4.6.
385 Subsequent circumferential bending moment plots are calculated using the strains readings
386 measured from the larger load pad tests.

387 **4.3 Impact of voids**

388 Figure 9 shows a plot of bending moment around the circumference for the intact pipe
389 with type 2 installation (specimen 6) versus the pipe with the small void and type 3 installation
390 (specimen 4) at 113 kN (25.5 kips) of surface load. Although an intact pipe with type 3
391 installation was tested (specimen 2), the strain sensors on that pipe malfunctioned meaning that
392 moment values could not be calculated. However, since the bedding factors are intended for a
393 pipe with type 2 installation, it is also informative to compare the response of the deteriorated
394 specimen to an intact specimen with proper soil support (specimen 6).

395 From Figure 9, it can be seen that the moments in specimen 4 are greater than the
396 moments in specimen 6. The most significant increase in moments is seen at the invert where the

moments have increased by approximately 70%. This result is to be expected for two reasons: the difference in soil compaction and the presence of the small erosion void. Both of these factors result in the soil surrounding pipe specimen 4 providing much lower lateral earth pressures on the pipe, so that bending moments increase substantially. This may have significant implications for the assessment of pipes with erosion voids next to them as they can potentially have less than half their expected capacity. Figure 9 also shows the maximum bending moment at the invert of specimen 4 with erosion void has shifted from the invert towards the location of the small void. This result is logical since the lack of soil on this side of the pipe likely produced greater transfer of vertical forces to that side of the pipe above and below the void, coupled with the reductions in lateral earth pressures. Results from the larger void test (specimen 5) are not presented in this paper as the fibre optics failed during the tests.

Assuming a liner elastic response prior to cracking (discussed in section 4.6), the larger void test (specimen 7a) results, from the smaller load pad test, were scaled from 50 kN ($F_H$ = 28.42 kN/m) to 80.76 kN ($F_H$ = 45.9 kN/m) and are presented in Figure 10.

From Figure 10, it can be seen that the moments in specimen 7a are greater than the moments in specimen 6. The most significant increase in moments is seen at the invert where the moments have increased by approximately 26%. It must be noted that the moments plotted in Figure 10 are extrapolated from the moment values measured at 50 kN load under the small load pad.

### 4.4 Impact of grouting

Figure 11 shows a comparison of grouted small void (specimen 3) results and intact soil (specimen 6) results for 113 kN (25.5 kips) applied to the larger loading pad. Again in this case,

since the bedding factors are intended for a pipe with type 2 installation, the response of the rehabilitated specimen has been compared to an intact specimen with proper soil support (specimen 6).

From Figure 11, it can be seen that once the small void was filled with grout, the results show a decrease in the bending moments (especially on the side of the grouted void and compared to the voided condition). For example, there was a 25% decrease in moments at the haunch (grouted void side) and an approximate 10% decrease at the invert between the repaired (grouted void) and the unrepaired (voided condition).

To investigate the implications of grouting the voids further, circumferential bending moments were compared between the grouted large void (specimen 7b) at $F_H$ = 45.9 kN/m and the intact soil (specimen 6) in Figure 12.

Figure 12 shows the extrapolated moment distributions in specimen 7b (grouted large void) and specimen 6 (intact soil) for $F_H$ = 45.9 kN/m. Further reduction in the overall bending moment can be seen compared to the grouted small void condition. Soil collapse was observed at surface loads greater than 100 kN (22.5 kips) for specimen 7b resulting in a change in the cover depth and the test was terminated. The probable cause of this ground failure was because the grout did not completely fill the large void, and so the soil directly under the wheel pad moved into some of the remaining void.

Based on the results of the two grouted void tests, it can be speculated that grouting an erosion void will result in the overall improvement of the system capacity versus not filling the erosion void. However, it should be noted that level of compaction of the surrounding soil also plays a major role in the distribution of surface loads to the soil-pipe system. For example, the

grouted large void (90-95% Standard Proctor compaction level) showed comparable responses to the intact soil test (90-95% Standard Proctor compaction level), while the grouted small void (80-85% Standard Proctor compaction level) showed an improvement in the overall response of the system but did not restore the original moment distribution in the pipe. The role of compaction is explored further in the next section.

### 4.5 Pipe cracking responses and linearity

The maximum load limits were either cracking in the pipes on the tension side of the pipe walls or soil collapse (especially in the large void tests).

The maximum load test results from the buried pipe tests are provided in Table 1. From Table 1, it can be seen that specimen 6 (90-95% Standard Proctor compaction level) cracked at the highest load, followed by the grouted small void test (specimen 3), the small void test (specimen 4), and the intact soil test with 80-85% Standard Proctor compaction level (specimen 2). Table 1 also shows that soil collapse was observed in the grouted large void and large void tests at low surface loads. However, it was observed that the grouted large void (specimen 7b) was not completely filled with grout when the pipe was excavated; hence, the presence of voids could have led to a premature failure in this case. It should be noted that the soil surfaces in these tests were unpaved and soil failure might be observed at higher loads if the surface was paved.

Figure 13 shows the vertical and horizontal change in diameter with increasing surface loads as measured using the linear potentiometers (LP's).

From this figure, it can be seen that the overall changes in diameter are very small, although after cracking, the changes in diameter begin to increase in a non-linear fashion. These

results demonstrate how buried rigid pipes have initial stiffness (i.e. deformation under load) that is dominated by the flexural rigidity of the pipe (see Moore, 2001), with almost identical deformations for different kinds of soil support. However, the bending moments that develop and which control the cracking loads depend heavily on the soil conditions. Figure 14 presents the bending moment in the pipes at (a) the crown and (b) the invert as a function of applied load at the surface for all the pipes for which strain data was available (excluding the D-load test).

Figure 14 shows an approximately linear increase in crown and invert bending moments as a function of applied loads, prior to cracking. Hence, the extrapolated moment values for specimen 7b are considered to be acceptable.

### 4.6 Modified bedding factors

As noted in section 2.3, the Bedding factor ($B_f$) can be defined as a measure of the performance of a buried pipe relative to the same pipe tested in a D-load test (unburied). It can be calculated using two approaches. Firstly, bedding factor is normally defined as the ratio between loads per unit length that produce the same amount of bending moment for the buried and D-load conditions, McGrath and Hoopes (1998) (Equation 6).

$$B_f = \frac{\text{Load per unit length for buried pipe}}{\text{Load per unit length for D - load}} \quad (6)$$

Alternatively, for a buried pipe system that is responding linearly, bedding factor can be expressed as the ratio of moments for the same vertical load per unit length (Equation 7).

$$B_f = \frac{\text{Moment per force per unit length for D - load}}{\text{Moment per surface force per unit lenth for buried pipe}} \quad (7)$$

Therefore, bedding factors obtained from equation 7 will be used in this section as a convenient method to quantify the support provided by the backfill to the pipes. Table 2 shows bedding factor calculated based on equations 6 and 7 for 50 kN (11.2 kips) surface load and at cracking loads respectively using the moments at the invert. When calculating the load spreading in the vertical direction to the pipe crown (i.e. the cover height), live load distribution factors (LLDF) of 1.15. According to AASHTO LRFD (2012), the LLFD value is 1.15 based on the backfill (i.e. select-granular soils). A comparison is also made between the results when the loads were applied using the small loading pad (service load pad) and large loading pad (maximum load test pad). The minimum live load bedding factor specified by AASHTO LRFD (2016) (Table 12.10.4.3.2c-1) for a 0.9 m diameter pipe with 0.9 m of cover is 2.2. However, the buried pipes did not reach the critical crack width of 0.25 mm before failure of the ground surface occurred.

Table 2: Modified bedding factor ($B_f$) using measured moments and cracking loads

| **Specimen** | **Test description** | **Average $B_f$ (Equation 6)** | | **$B_f$ at first crack (Equation 7)** |
|---|---|---|---|---|
| | | **Small pad at 50 kN** | **Large pad at 50 kN** | |
| | | LLDF = 1.15 | LLDF = 1.15 | LLDF = 1.15 |
| 2 | Intact soil (80-85%) | A | A | 1.4 |
| 3 | Grouted small void (80-85%) | 1.6 | 2.0 | 1.6 |
| 4 | Small void (80-85%) | 1.6 | 1.8 | 1.4 |

| | | | | |
|---|---|---|---|---|
| 5 | Large void (80-85%) | A | A | B |
| 6 | Intact soil (90-95%) | 2.9 | 3.2 | 2.6 |
| 7a | Large void service load (90-95%) | 1.4 | C | C |
| 7b | Grouted large void (90-95%) | 2.4 | 2.4 | B |
| AASHTO LRFD (2016) minimum requirement | | | 2.2 | |

Notes: A. Optical fibre broke on this sample so moment values are not available

B. Soil collapse was observed

C. Test was not conducted to failure (critical cracking of pipe or soil collapse)

All the specimens with voids have bedding factors that are lower than the minimum requirement as does the specimen with the grouted small void. The intact soil specimen has the highest bedding factors and it is well above the required value of 2.2, which makes sense since the bedding factor is meant to lead to conservative designs. Table 2 also clearly shows that as the backfill support decreases, the lower the cracking load and therefore the lower the bedding factor value. Figure 15 shows how bedding factors change with load steps from 25 kN to 113 kN in the maximum load test tests with LLDF = 1.15.

It can be seen in Figure 15 that the bedding factors calculated using crown moments and load spreading to the crown of buried pipes result in much higher values. This was because the crown moment from the D-load test was higher than those at other critical locations as it

approached the cracking limit state on the tension side first as noted earlier. Bedding factors calculated using invert moments and load spreading to the invert of buried pipes result in values where only the intact soil and the grouted large void are greater than the minimum AASHTO specified design value of 2.2 (Figure 16). However, in both cases the general trend seen is that the intact soil (specimen 6) has the highest bedding factor, followed by the grouted large void (specimen 7b), grouted small void (specimen 3), and finally the small void (specimen 4). At a few load levels (loads greater than the maximum AASHTO design service load (105 kN)), the grouted small void results are greater than the AASHTO design value. This suggests that the experimental determination of the bedding factor is load dependent. It is also suggests that the bedding factor may be very conservative for the design of non-deteriorated pipes.

## 5.0 Conclusions

Slow deterioration of pipes can contribute to the formation of erosion voids in the backfill due to fluid leaking both into and out of the pipe. The presence of these voids corresponds to a lack of soil support that results in uneven load spreading in the ground. No previous full-scale experiments have explored the effects of voids beside rigid pipes. The tests presented in this paper represent the first full-scale, controlled laboratory tests investigating the effect of erosion voids adjacent to buried concrete pipes, and the results provide a unique insight into the effects of these voids on rigid pipe behaviour and the potential impact of low strength grout as a remedial measure. The tests involved investigating and quantifying the effect of live loads on the performance of 0.9 m (36 in.) diameter, Class III, concrete pipes buried with a 0.9 m (36 in.) cover depth, with erosion voids simulated on one side of the pipe.

A summary of the pipe responses to surface live loads are given below:

a. Cracking was observed in most of the tests, although burial in soil with high compaction and high lateral soil support (i.e. intact soil test with compaction to 90-95% of maximum density from a Standard Proctor test) ensures cracking at very high loads. When erosion voids are present beside the pipe, there is a reduction in the soil support and the pipe takes on more loads (arching). Hence, the pipes crack at substantially lower surface loads. This is clear from the results, where the test on pipe in intact soil with density corresponding to 90-95% Standard Proctor compaction) cracked at the highest load 525 kN, followed by grouted small void at 308 kN, followed by small void test at 277 kN, and intact soil (80-85% Standard Proctor compaction) at 273 kN.

b. The presence of erosion voids resulted in an overall increase in bending moment with the invert moments being affected the most (e.g., 70% change in the invert moment between the intact soil result and the small void result and a 26% change in the invert between the intact soil result and the extrapolated large void results). This validates the computer analyses of Tan and Moore (2007), where an overall increase in bending moments was also observed for erosion voids located at the pipe springline.

c. The test featuring larger voids also showed soil collapse as the dominant failure mechanism. It was observed that increasing the contact angle of the erosion voids to the pipe eventually lead to a change in failure mode, so that surface soil collapse became dominant (under unpaved roads). This shows that erosion voids can be highly undesirable, given that they can create unstable conditions that jeopardize the roadway overhead.

d. On exhumation of the grouted large void, it was observed that the grout did not fully fill the void, and it appears that the soil directly under the loading pad collapsed into the

555 remaining void. This was the case even though a comparison of the strains and bending
556 moment readings demonstrated that the pipe responses were very similar to those for the
557 intact soil condition.
558 e. A small difference in the degree of compaction, for example type 2 installation for intact
559 soil (specimen 6) and type 3 installation of intact soil (specimen 2) lead to significant
560 changes in the bedding factor results as seen in the calculated cracking bedding factor
561 values 2.6 and 1.4 respectively (46% reduction).
562 f. Comparisons between the large plate bedding factor values for the pipes show that the
563 intact backfill soil provided the highest bedding factor, followed by grouted large void
564 (approximately 22% reduction), grouted small void (approximately 36% reduction), and
565 ultimately small void (approximately 39% reduction).

566 **6.0 Acknowledgments**

567 This project was funded by support provided by the Natural Sciences and Engineering
568 Research Council of Canada (NSERC) through a Strategic Research Grant to Drs. Moore and
569 Hoult. The GeoEngineering Laboratory and test facilities used were provided through grants
570 from the Canada Foundation for Innovation, NSERC, the Province of Ontario, and support from
571 Queen's University. Dr. Chapman's involvement in the project as a Visiting Scholar was funded
572 with generous support from Golder Associates in partnership with the GeoEngineering Centre at
573 Queen's – RMC. Samples of reinforced concrete pipe were provided by M-CON of Ottawa and
574 made possible by Mr. Paul Imm of the Ontario Concrete Pipe Association. Portland cement was
575 donated by Lafarge North America Incorporated. Thanks also to Danny Salvo of Euclid Canada
576 who provided his expertise, the Aerix aerating agent, and the foam generating equipment. The

577 essential and extraordinary contributions to the experimental work made by Graeme Boyd, Eric
578 Poon, Eric Jeffery, Sankranti Patel and Brian Westervelt are also gratefully acknowledged.

579 Any opinions, findings, conclusions, or recommendations expressed in this article are
580 those of the authors and do not necessarily reflect the views of the sponsors.

581 **7.0 References**

582 AASHTO (2012). LRFD Bridge Design Specification, 6th Edition, American Association of
583 State Highway and Transportation Officials, Washington D.C.

584 AASHTO (2013). AASHTO LRFD Bridge Design Specifications, 6th Edition, 2013 Interim
585 Revisions. AASHTO, Washington, D.C.

586 AASHTO (2016). AASHTO LRFD Bridge Design Specifications, 7th Edition, 2015 and 2016
587 Interim Revisions. AASHTO, Washington, D.C.

588 American Society of Testing and Materials (ASTM)(2016). C497-16a, Standard Test Methods
589 for Concrete Pipe, Manhole Sections, or Tile. ASTM International, West Conshohocken, PA.

590 ASTM C76-11 (2011). Standard Specification for Reinforced Concrete Culvert, Storm Drain,
591 and Sewer Pipe. ASTM International, West Conshohocken, PA.

592 ASTM D6938-10 (2010). Standard Test Method for In-Place Density and Water Content of Soil
593 and Soil Aggregate by Nuclear Methods (Shallow Depth), ASTM International, PA.

594 Balkaya, M., Moore, I. D., & Sağlamer, A. (2012). Study of non-uniform bedding due to voids
595 under jointed PVC water distribution pipes. Geotextiles and Geomembranes, 34, pp. 39-50.

596 Balkaya, M., Moore, I. D., & Sağlamer, A. (2013). Study of non-uniform bedding support under
597 continuous PVC water distribution pipes. Tunnelling and Underground Space Technology, 35,
598 pp. 99-108.

599 Becerril García, D. & Moore, I.D. (2013). Behavior of Bell and Spigot Joints in Buried
600 Thermoplastic Pipelines, Transportation Research Record, Vol. 2332, pp. 29-40.

601 Becerril García, D. & Moore, I.D. (2014). Behavior of Coupling Band Joints in Buried
602 Corrugated Steel Culverts, Journal of Geotechnical and Geoenvironmental Engineering, ASCE,
603 Vol. 140, No. 2, 04013014.

604 Becerril García, D., & Moore, I. D. (2014). Behaviour of bell and spigot joints in buried
605 reinforced concrete pipelines 1. Canadian Geotechnical Journal, 52(5), pp. 609-625.

606 Brachman, R.B., Mak, A.C. and Moore, I.D. 2010. Ultimate limit state of a deep-corrugated
607 large-span box culvert, Transportation Research Record, No. 2201: 55-61.

608 Cheng, L., Draper, S., & An, H. (Eds.). (2014). Scour and Erosion: Proceedings of the 7th
609 International Conference on Scour and Erosion, Perth, Australia, 2-4 December 2014. CRC
610 Press.

611 El-Taher, M., & Moore, I. (2008). Finite element study of stability of corroded metal
612 culverts. Transportation Research Record: Journal of the Transportation Research Board, (2050),
613 pp. 157-166.

614 Heger, F. J. (1962). A theory for the structural behavior of reinforced concrete pipe. Doctoral
615 dissertation, Massachusetts Institute of Technology.

616 Lay, G. R., & Brachman, R. W. I. (2013). Full-scale physical testing of a buried reinforced
617 concrete pipe under axle load. *Canadian geotechnical journal*, *51*(4), pp. 394-408.
618 (https://doi.org/10.1139/cgj-2012-0256)

619 Lambe, T. W., Whitman, R. V., 1979. Soil Mechanics, SI Version. New York, John Wiley &
620 Sons: publisher.

621 MacDougall, K. (2014). Behaviour and design of reinforced concrete pipes (Master's thesis).
622 Retrieved from Queen's University. (http://hdl.handle.net/1974/12244)

623 MacDougall, K., Hoult, N. A., & Moore, I. D. (2016). Measured Load Capacity of Buried
624 Reinforced Concrete Pipes. *ACI Structural Journal*, *113*(1), 63-73

625 McGrath, T. J. and Hoopes, R. J., (1998) "Bedding Factors and E' Values for Buried Pipe
626 Installations Backfilled with Air-Modified CLSM," The Design and Application of Controlled
627 Low-Strength Materials (Flowable Fill), ASTM STP 1331, A. K. Howard and J. L. Hitch, Eds.,
628 American Society for Testing and Materials.

629 McGrath, T.J., Selig, E.T., Webb, M.C., Zoladz, G.V., 1999. Pipe Interaction with the Backfill
630 Envelope, FHWA-RD-98-191. US Department of Transportation, Federal Highway
631 Administration.

632 Moore, I. D. (2008). Studies of buried pipe behaviour. Structures and Granular Solids: From
633 Scientific Principles to Engineering Application, 77-85.

634 Moore, I. D. (2008, April). Assessment of damage to rigid sewer pipes and erosion voids in the
635 soil, and implications for design of liners. In North American Society for Trenchless
636 Technology, No-Dig Conference & Exhibition.

637 Moore, I. D., Garcia, D. B., Sezen, H., & Sheldon, T. (2012). Structural design of culvert
638 joints (No. NCHRP Project 15-38).

639 Peter and Moore (2018). Effects of an erosion void on deteriorated metal culverts at the service
640 loads and its effect when repaired for service and ultimate limit loads. under review for the J. of
641 Pipeline Engineering Systems and Management, ASCE.

642 Petersen, D.L., Nelson, C.R., Li, G., McGrath, T.J. and Kitane, Y. (2010). NCHTP Report 647:
643 Recommended Design Specifications for Live Load Distribution to Buried Structures.
644 Transportation Research Board, Washington, D.C.

645 Simpson, B., Hoult, N. A., & Moore, I. D. (2015). Distributed sensing of circumferential strain
646 using fiber optics during full-scale buried pipe experiments. *Journal of Pipeline Systems*
647 *Engineering and Practice*, *6*(4), 04015002.

648 Spasojevic, A. D., Mair, R. J., & Gumbel, J. E. (2007). Centrifuge modelling of the effects of
649 soil loading on flexible sewer liners. Géotechnique, 57(4), pp. 331-341.

650 Tan, Z. (2007). Nonlinear finite element study of deteriorated rigid sewers including the
651 influence of erosion voids. MASc thesis, Department of Civil Engineering, Queen's University.

652 Tan, Z. and Moore, I.D. (2007). Effect of backfill erosion on moments in buried rigid pipes,
653 Paper number TRB 07-2674. Transportation Research Board Annual Conference, Washington
654 D.C. January, 29pp.

655 White, D. J., Take, W. A., & Bolton, M. D. (2003). Soil deformation measurement using particle
656 image velocimetry (PIV) and photogrammetry. Geotechnique, 53(7), pp. 619-632.

657 Wang and Moore, (2015). Simplified design model for rigid pipe joints based on the two-pipe
658 approximation. Canadian geotechnical Journal, 52(5), pp. 626-637.

659 Young, O. C., & Trott, J. J. (1984). Buried rigid pipes: Structural design of pipelines. London:
660 Elsevier.

661

List of Tables

Table 1: Test details

Table 2: Modified bedding factor ($B_f$) using measured moments and cracking loads

List of Figures

Figure 1: D-load setup in the laboratory and a schematic of the loading arrangement (dimensions in m)

Figure 2: Elevation of specimens 2 and 3 (dimensions in metres)

Figure 3: Specimens 2 and 3 before backfilling

Figure 4: Specimens 4 and 5 (dimensions in metres)

Figure 5: Cross sectional view of the smaller and larger voids located on the outside of the buried pipe (dimensions in m)

Figure 6: Instrumentation used inside the reinforced concrete pipe

Figure 7: Loading pads: (a) AASHTO wheel pair for service load tests, (b) Larger pad for ultimate load test

Figure 8: Circumferential bending moment (kNm/m) in the D-load and intact soil test pipes (specimens 1 and 6 respectively)

Figure 9: Circumferential bending moment (kNm/m) in the small void and intact soil (specimens 4 and 6 respectively)

Figure 10: Extrapolated circumferential bending moment (kNm/m) in the large void and intact soil specimens (specimens 7a and 6 respectively)

682 Figure 11: Circumferential bending moment (kNm/m) in the intact soil and grouted small void
683 test pipes (specimens 6 and 3 respectively)

684 Figure 12: Circumferential bending moment (kNm/m) in the intact soil and grouted large void
685 test pipes (specimens 6 and 7b respectively)

686 Figure 13: Vertical and horizontal linear potentiometer (LP) movement vs load step

687 Figure 14: Bending moment as a function of applied load using large load pad: (a) crown, (b)
688 invert

689 Figure 15: 'Moment demand' bedding factors calculated considering load spreading to the crown
690 using an LLDF = 1.15 and a larger loading pad

691 Figure 16: 'Moment demand' bedding factors calculated considering load spreading to the invert
692 using an LLDF = 1.15 and a larger loading pad


Hanson
NC 2622-126 1058 CSA A257.2
960MM CL III 6 D TBA
2015 02 18

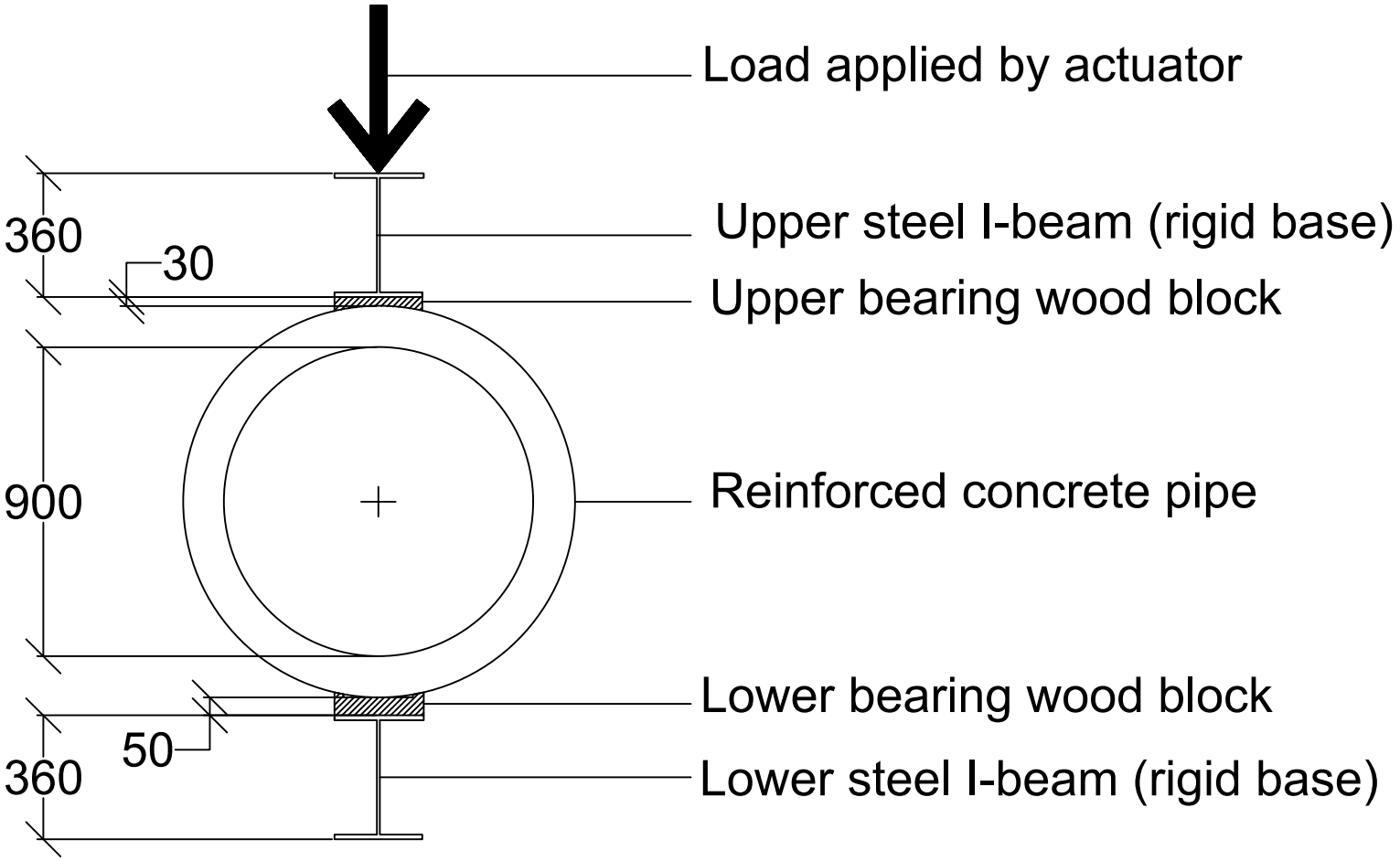
Load applied by actuator
360
30
Upper steel I-beam (rigid base)
Upper bearing wood block
900
Reinforced concrete pipe
Lower bearing wood block
50
360
Lower steel I-beam (rigid base)

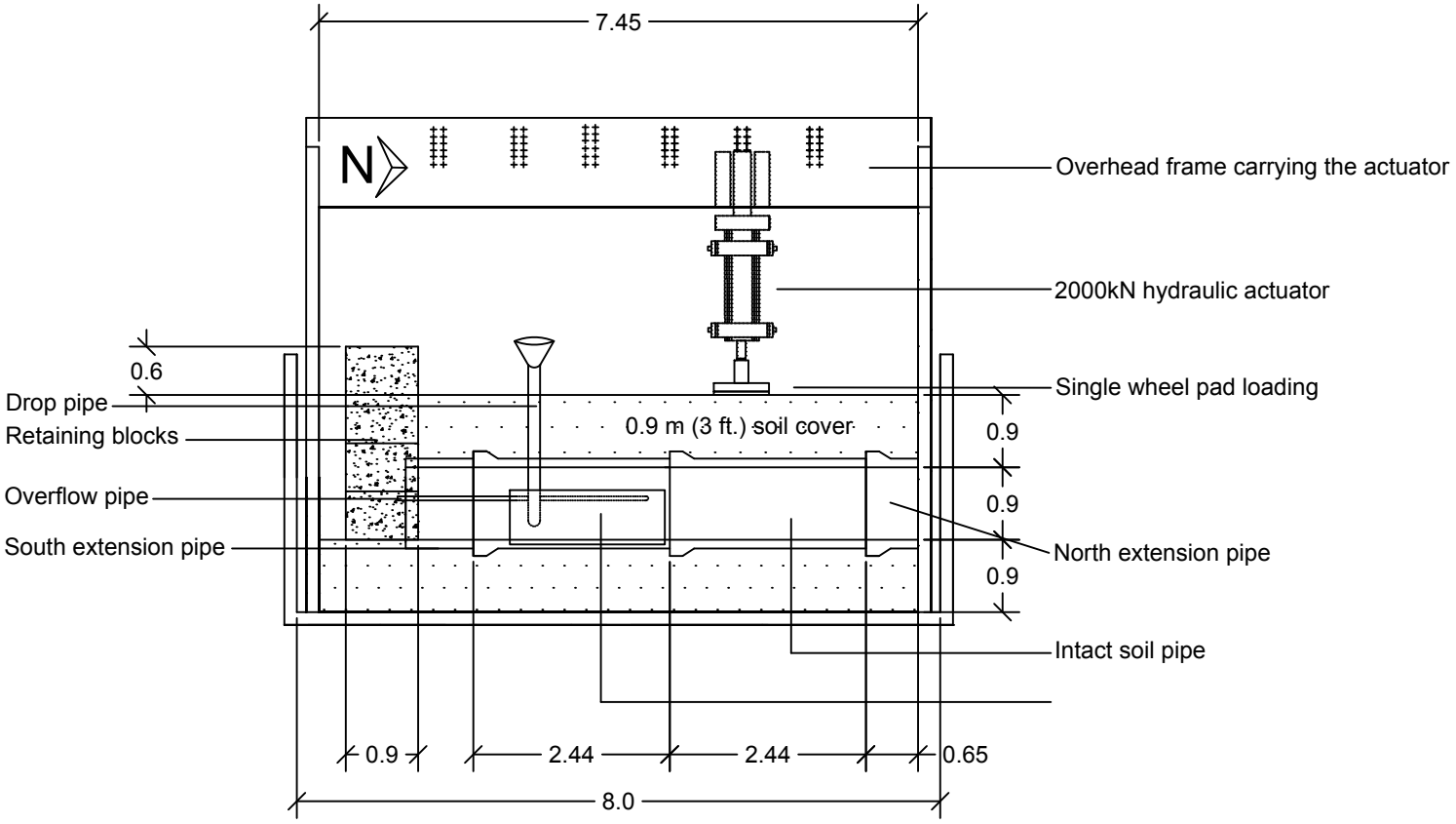
7.45
N
Overhead frame carrying the actuator
2000kN hydraulic actuator
0.6
Drop pipe
Retaining blocks
Overflow pipe
South extension pipe
Single wheel pad loading
0.9 m (3 ft.) soil cover
0.9
0.9
0.9
North extension pipe
Intact soil pipe
0.9
2.44
2.44
0.65
8.0

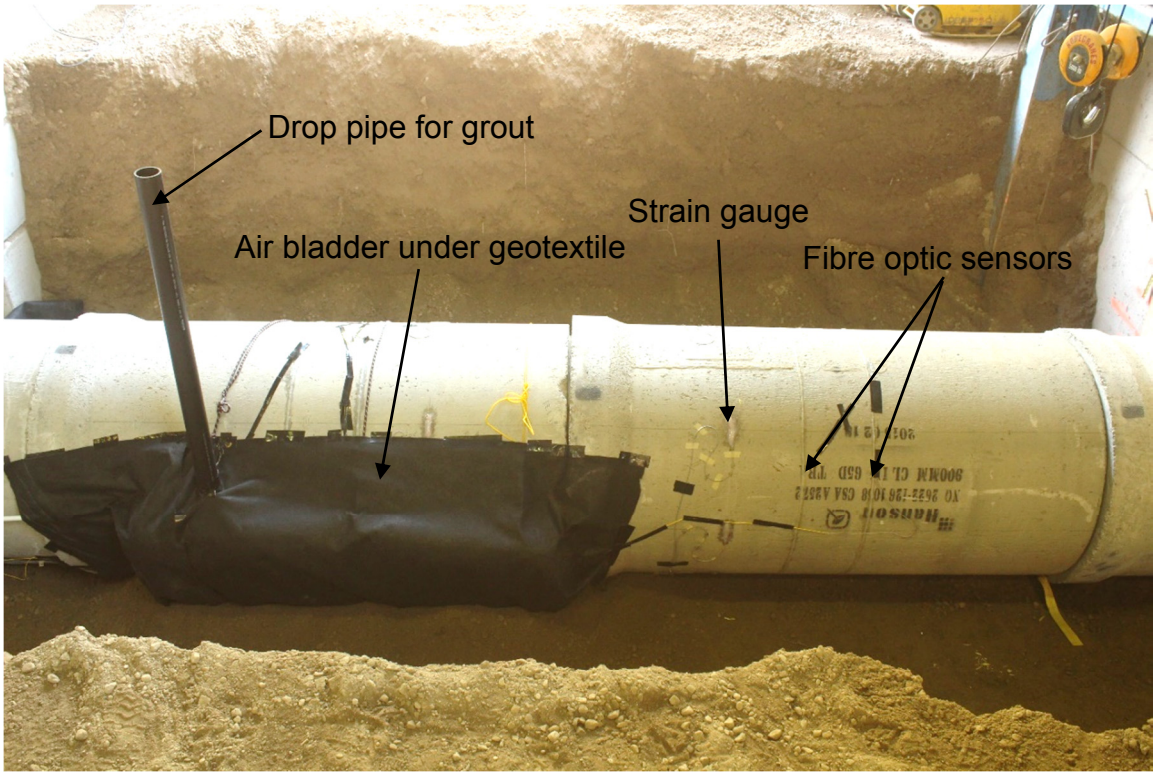
Drop pipe for grout
Air bladder under geotextile
Strain gauge
Fibre optic sensors

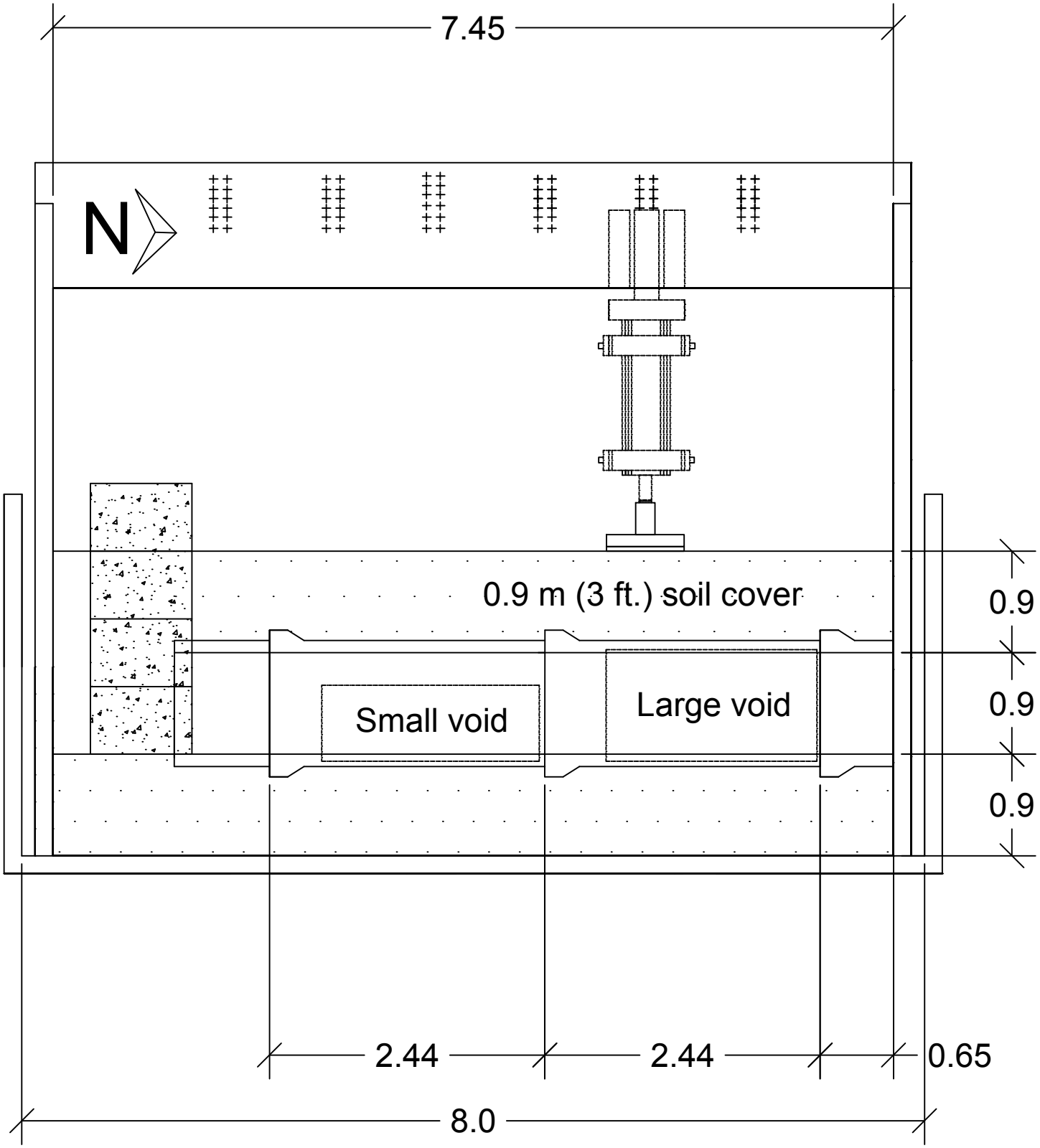
7.45
N
0.9 m (3 ft.) soil cover
Small void
Large void
0.9
0.9
0.9
2.44
2.44
0.65
8.0

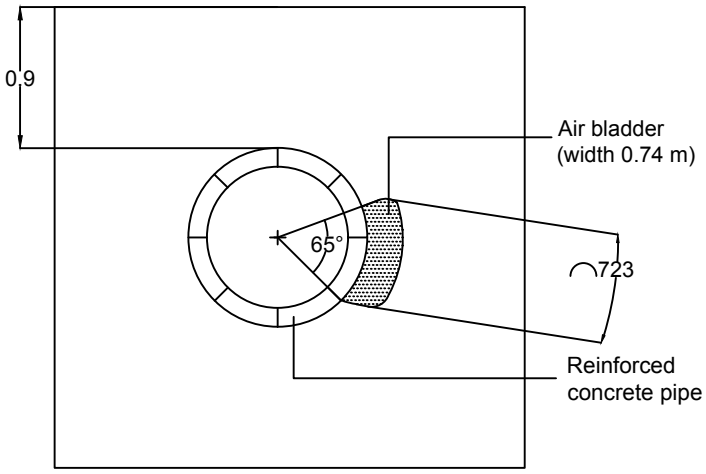
0.9
Air bladder
(width 0.74 m)
65°
723
Reinforced
concrete pipe

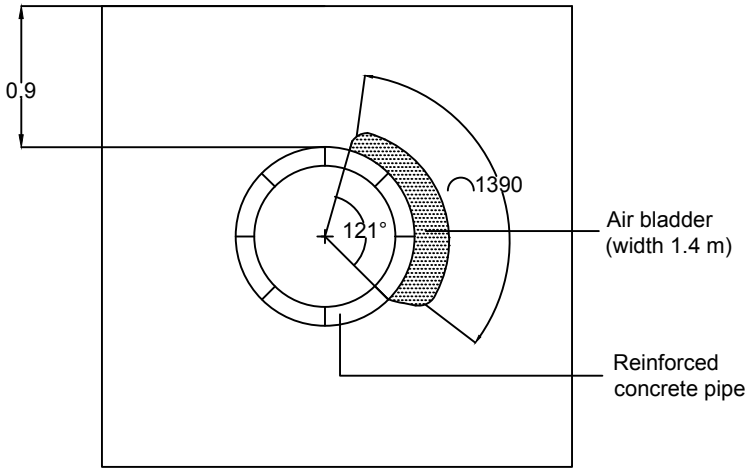
0.9
1390
121°
Air bladder
(width 1.4 m)
Reinforced
concrete pipe

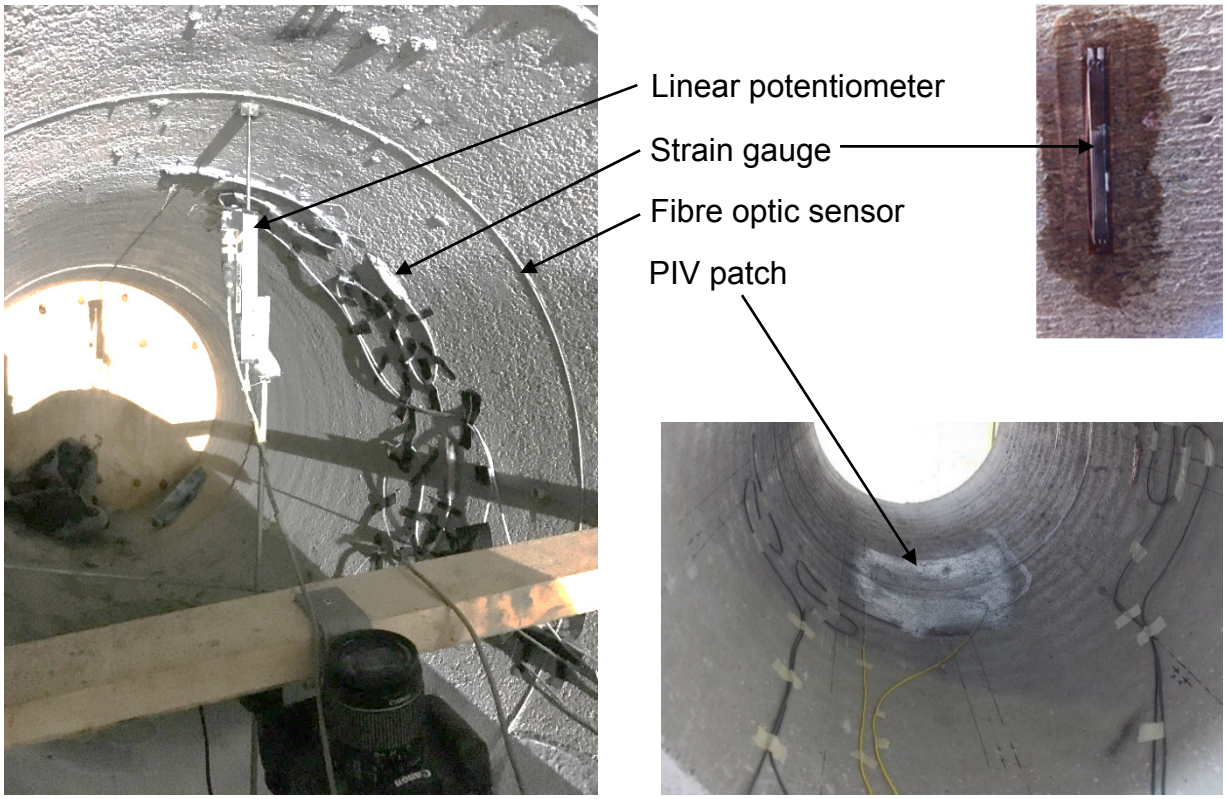
Linear potentiometer
Strain gauge
Fibre optic sensor
PIV patch

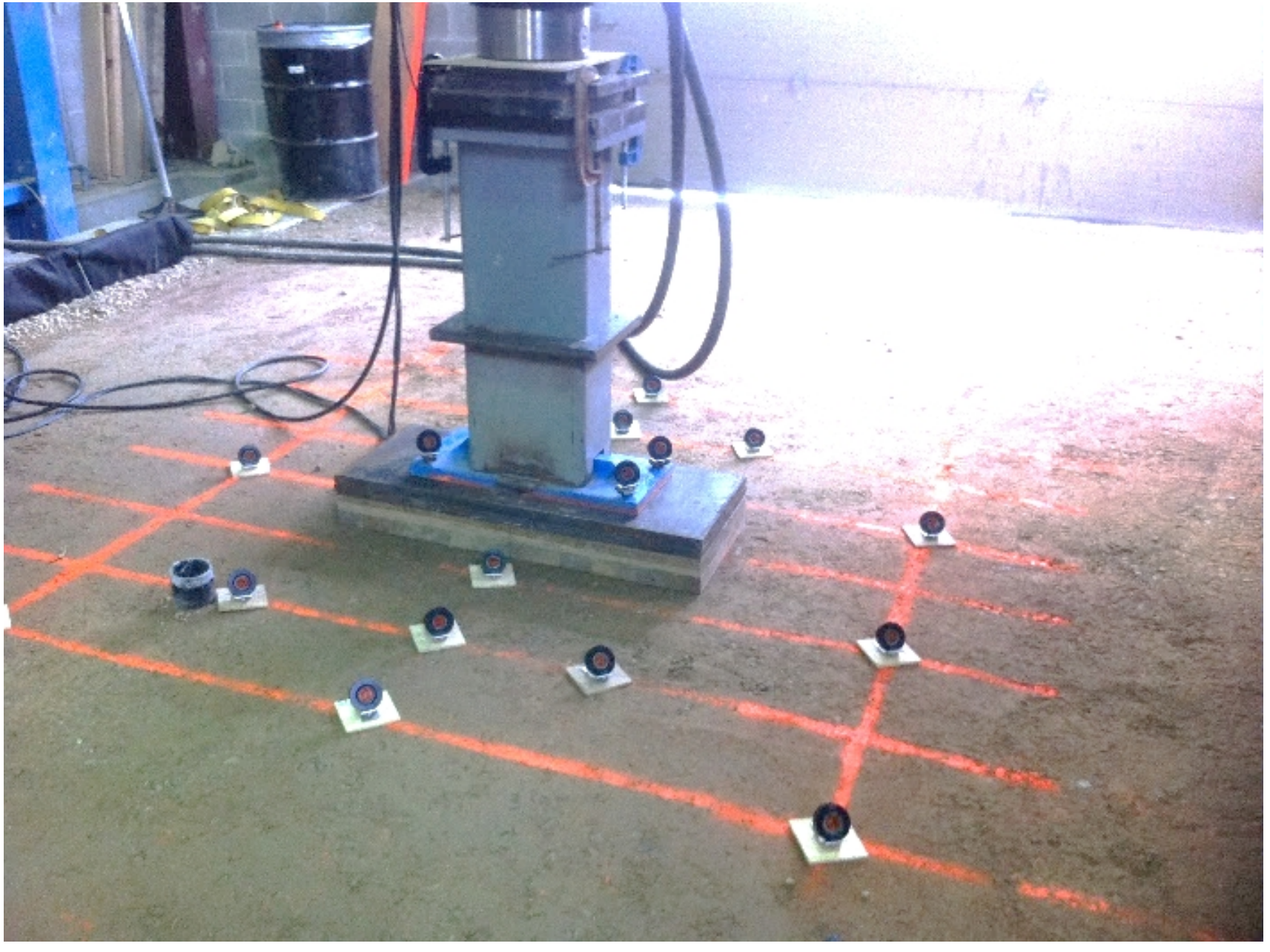

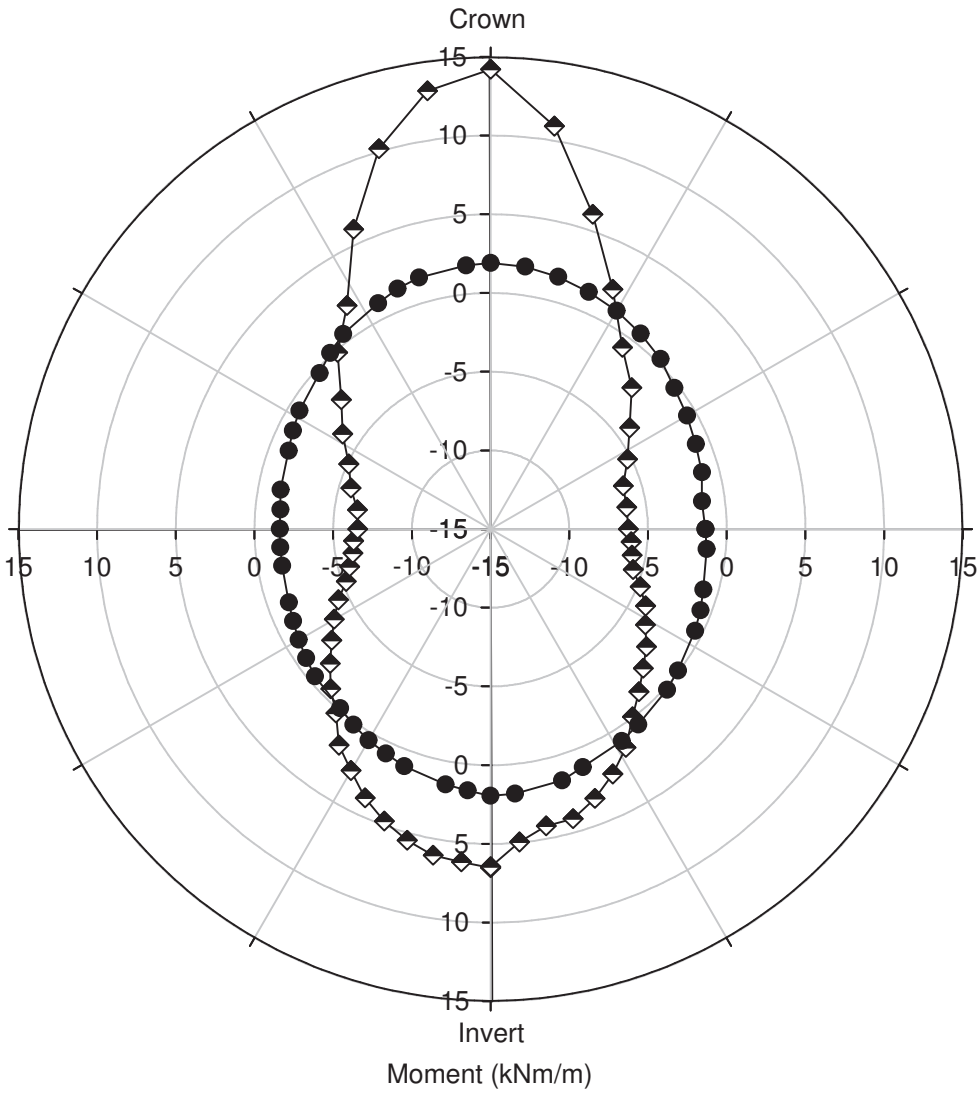


D-load (specimen 1) moment for $F_H$ = 45.9 kN/m

Intact soil (specimen 6) moment at 90-95% Standard Proctor for $F_H$ = 45.9 kN/m

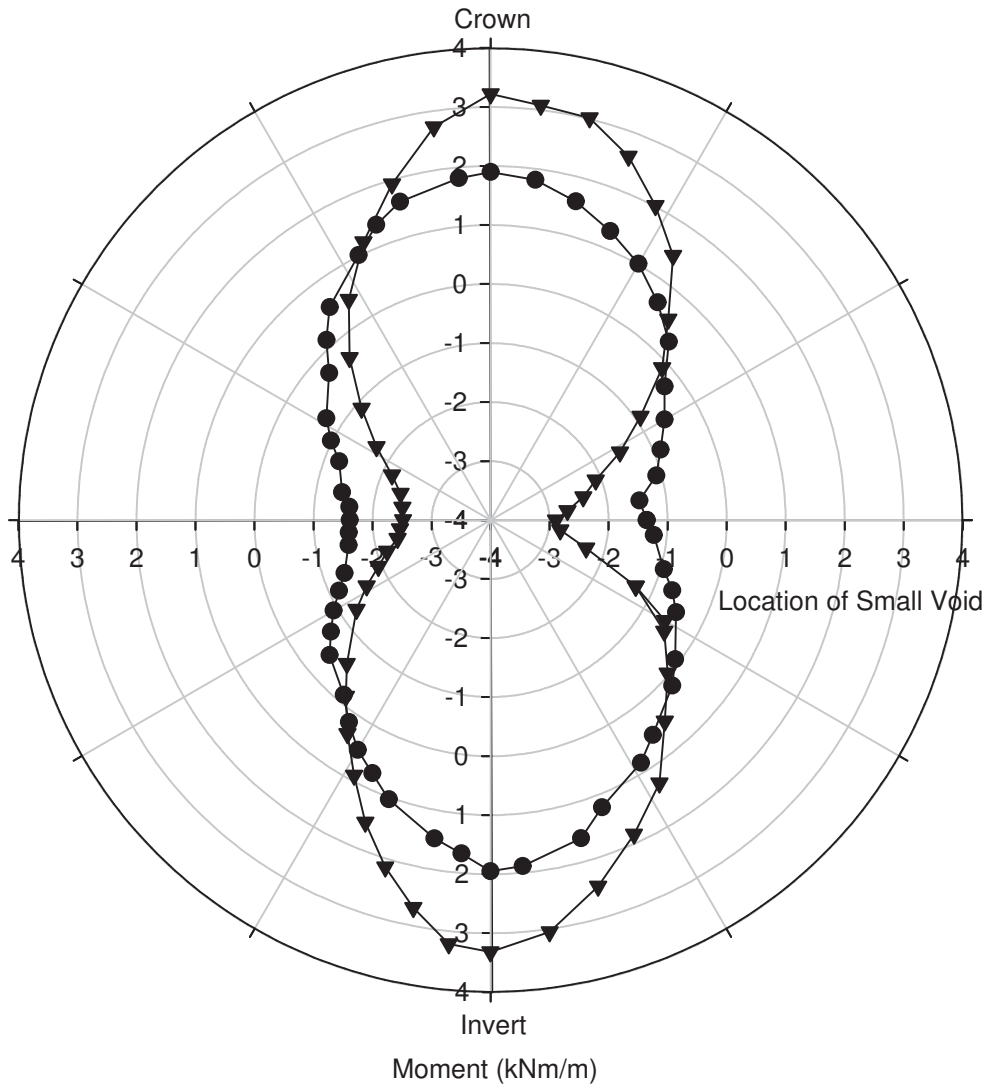


Small void (specimen 4) moment at 80-85% Standard Proctor for $F_H$ = 45.9 kN/m

Intact soil (specimen 6) moment at 90-95% Standard Proctor for $F_H$ = 45.9 kN/m

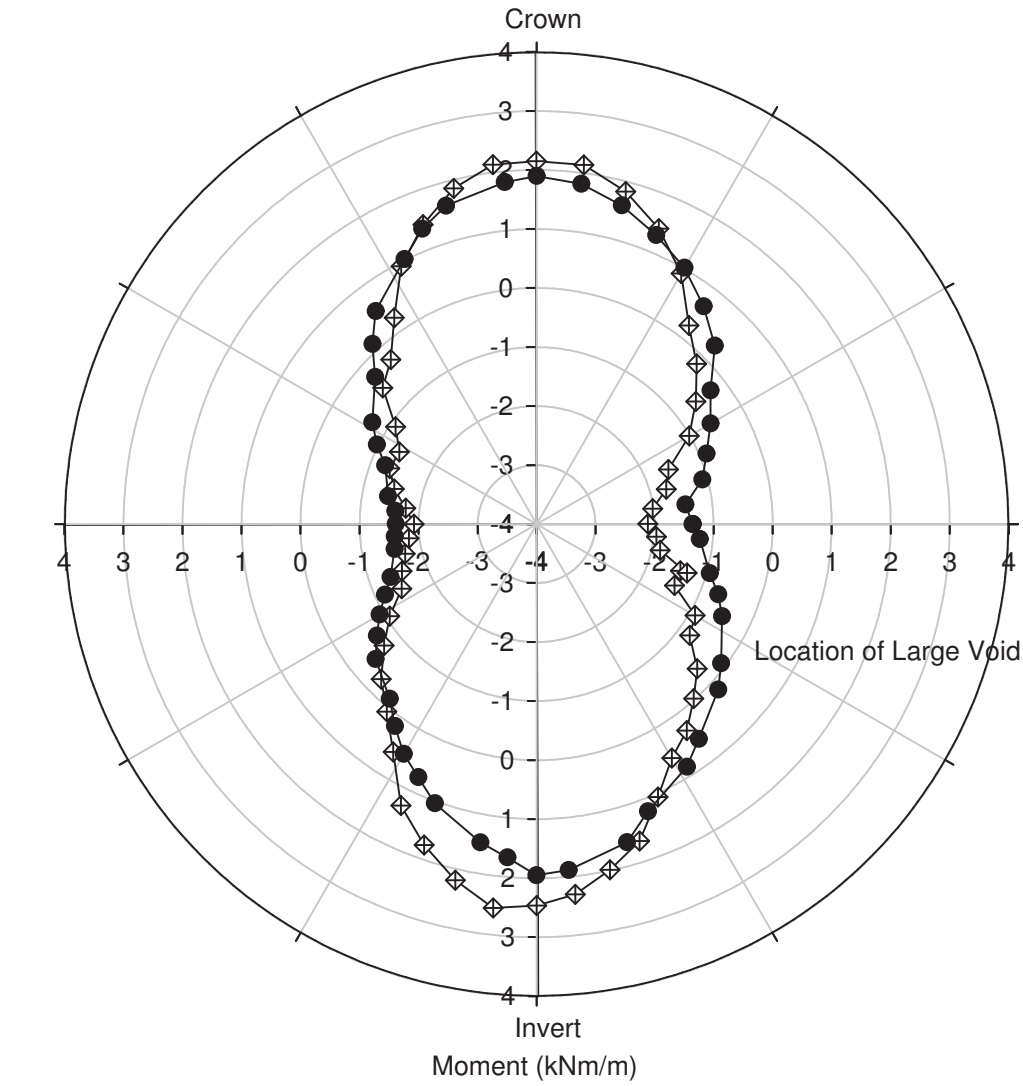


Large void (specimen 7a) moment at 90-95% Standard Proctor for $F_H$ = 45.9 kN/m

Intact soil (specimen 6) moment at 90-95% Standard Proctor for $F_H$ = 45.9 kN/m

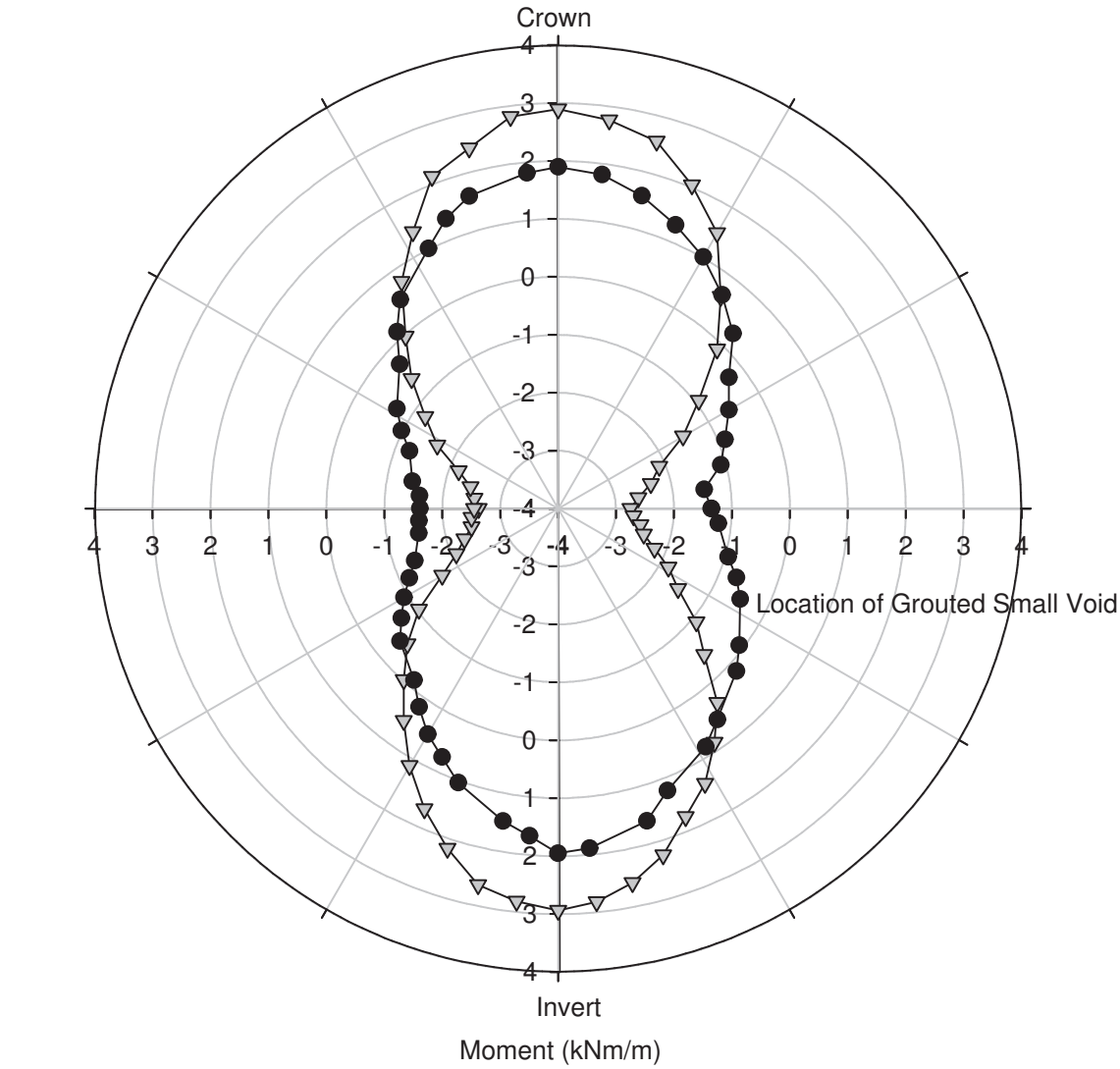


Grouted small void (specimen 3) moment for 80-85% Standard Proctor for $F_H$ = 45.9 kN/m

Intact soil (specimen 6) moment for 90-95% Standard Moment for $F_H$ = 45.9 kN/m

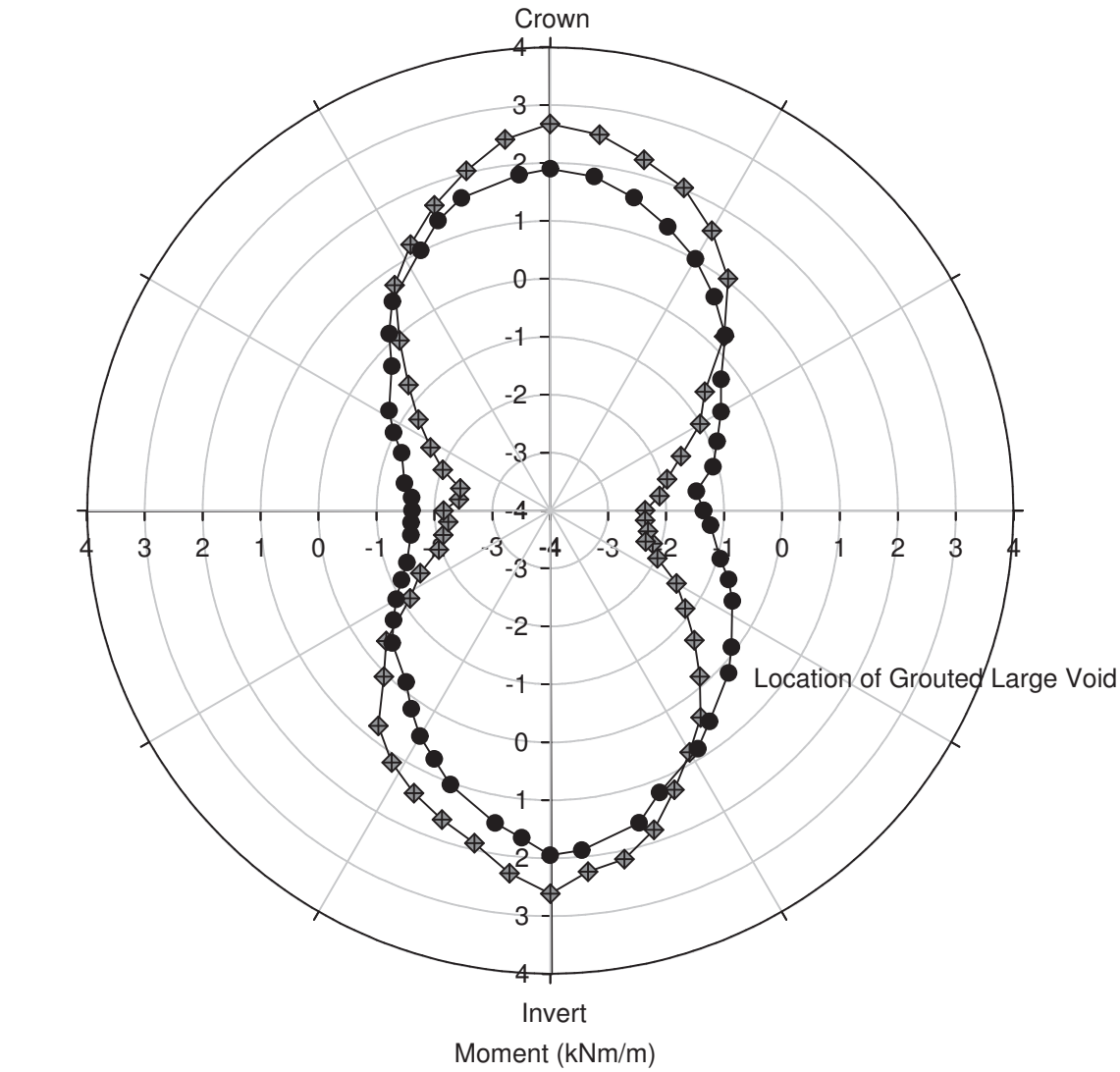


Grouted large void (specimen 7b) moment at 90-95% Standard Proctor for $F_H$ = 45.9 kN/m

Intact soil (specimen 6) moment at 90-95% Standard Proctor for $F_H$ = 45.9 kN/m

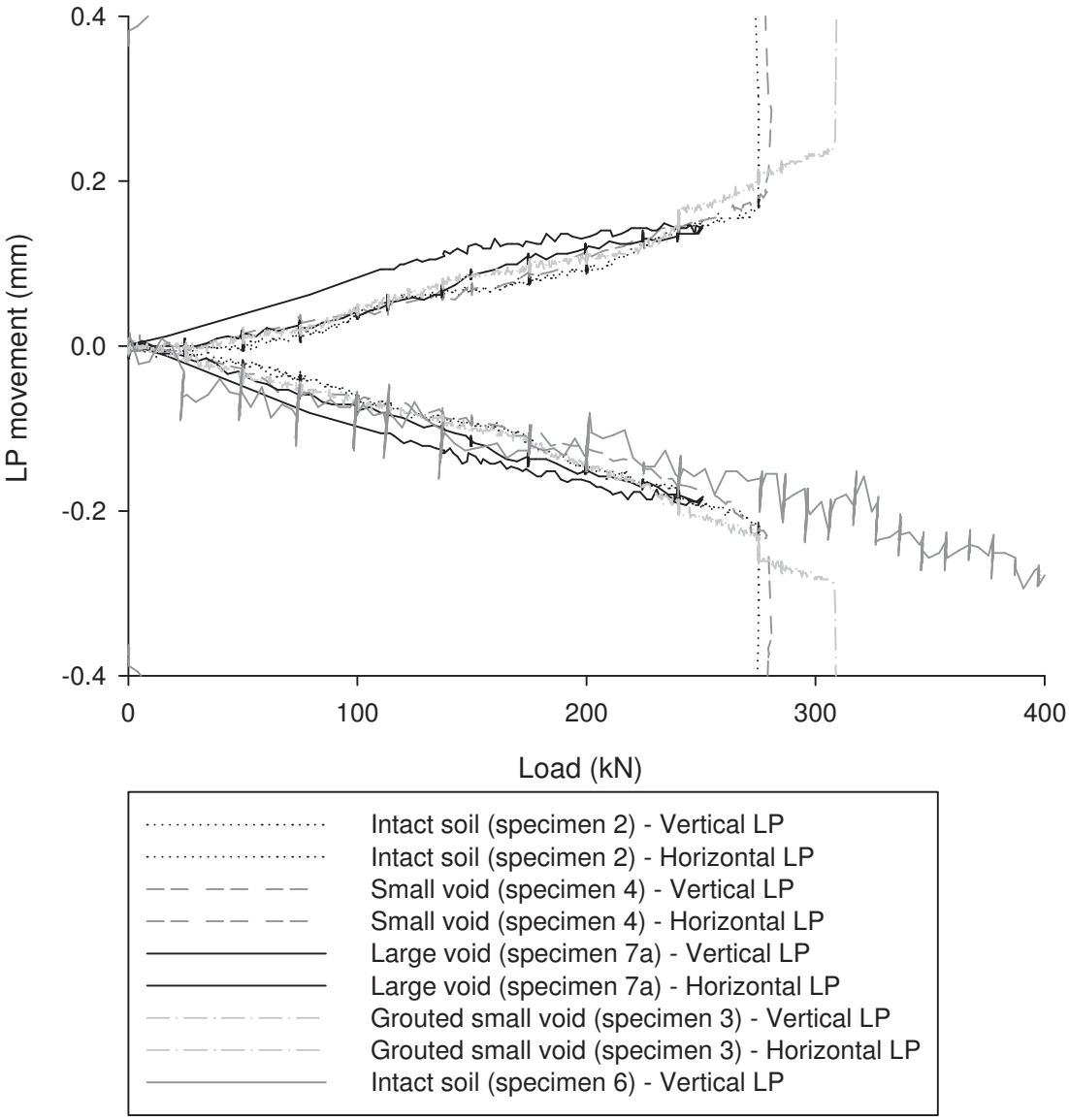
0.4
0.2
0.0
-0.2
-0.4
LP movement (mm)
0
100
200
300
400
Load (kN)
Intact soil (specimen 2) - Vertical LP
Intact soil (specimen 2) - Horizontal LP
Small void (specimen 4) - Vertical LP
Small void (specimen 4) - Horizontal LP
Large void (specimen 7a) - Vertical LP
Large void (specimen 7a) - Horizontal LP
Grouted small void (specimen 3) - Vertical LP
Grouted small void (specimen 3) - Horizontal LP
Intact soil (specimen 6) - Vertical LP

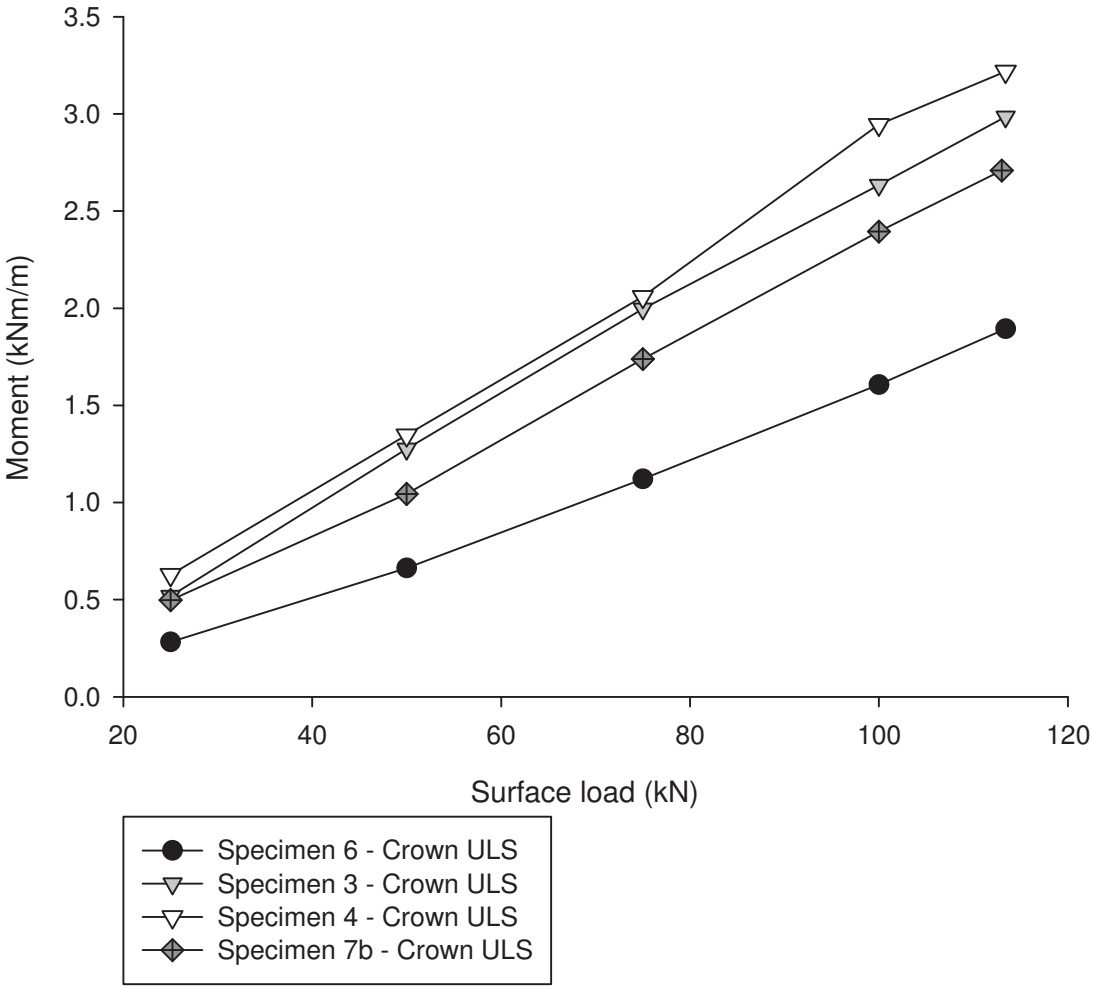
3.5
3.0
2.5
2.0
1.5
1.0
0.5
0.0
Moment (kNm/m)
20
40
60
80
100
120
Surface load (kN)
Specimen 6 - Crown ULS
Specimen 3 - Crown ULS
Specimen 4 - Crown ULS
Specimen 7b - Crown ULS

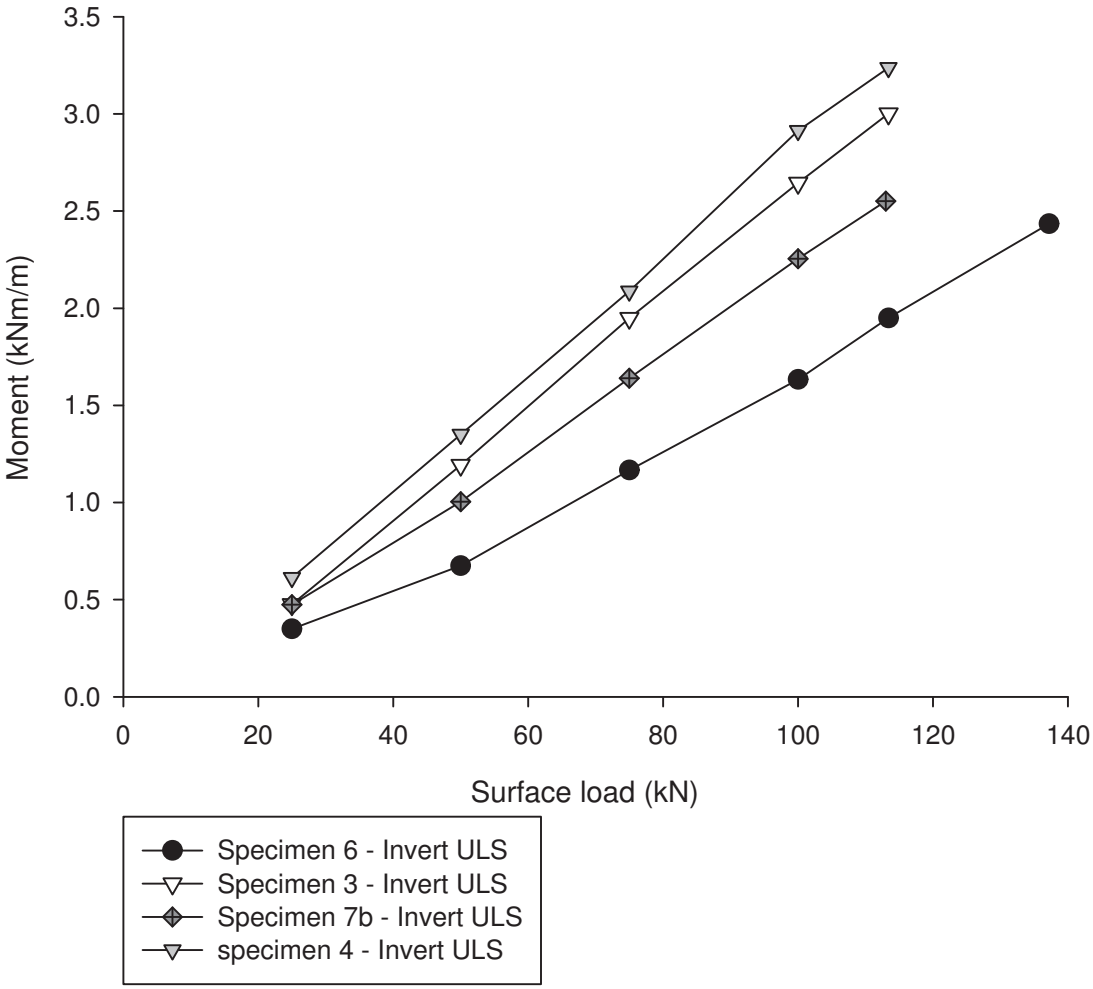
3.5
3.0
2.5
2.0
1.5
1.0
0.5
0.0
Moment (kNm/m)
0
20
40
60
80
100
120
140
Surface load (kN)
Specimen 6 - Invert ULS
Specimen 3 - Invert ULS
Specimen 7b - Invert ULS
specimen 4 - Invert ULS

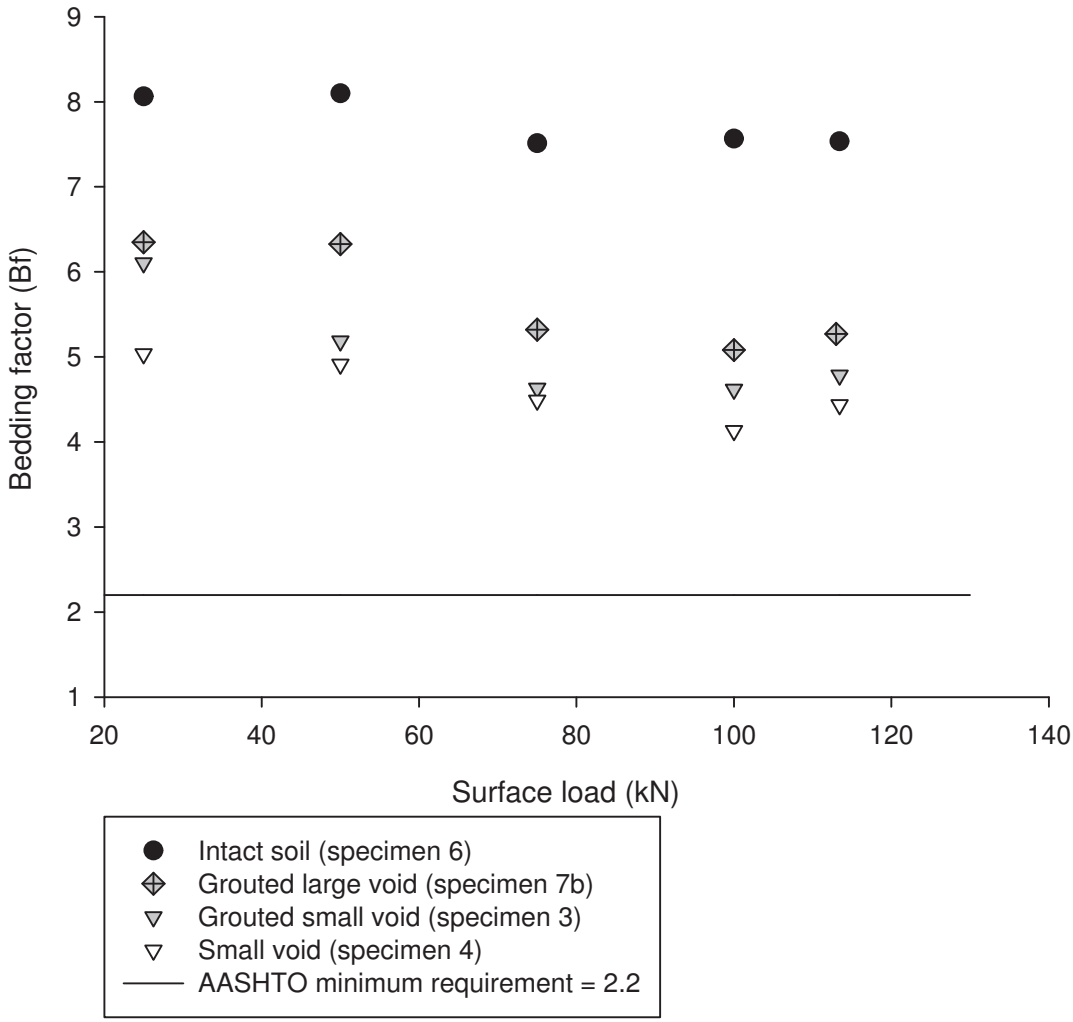
Bedding factor (Bf)
9
8
7
6
5
4
3
2
1
20
40
60
80
100
120
140
Surface load (kN)
Intact soil (specimen 6)
Grouted large void (specimen 7b)
Grouted small void (specimen 3)
Small void (specimen 4)
AASHTO minimum requirement = 2.2

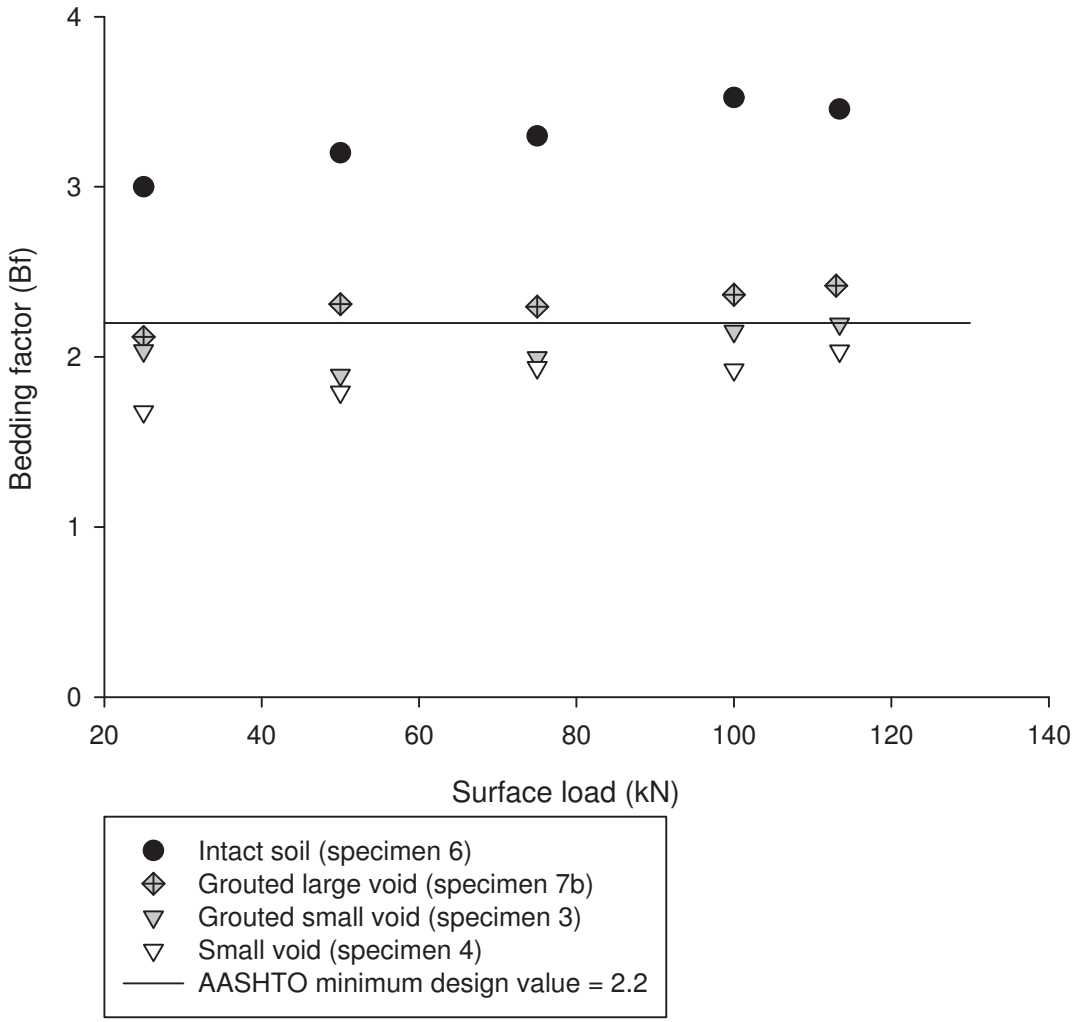
Bedding factor (Bf)
4
3
2
1
0
20
40
60
80
100
120
140
Surface load (kN)
Intact soil (specimen 6)
Grouted large void (specimen 7b)
Grouted small void (specimen 3)
Small void (specimen 4)
AASHTO minimum design value = 2.2